

Review

Micro-Channel Oscillating Heat Pipe Energy Conversion Approach of Battery Heat Dissipation Improvement: A Review

Xiaohuan Zhao, Yue Zhu and Hailiang Li *

Energy and Electricity Research Center, International Energy College, Zhuhai Campus, Jinan University, No. 206, Qianshan Road, Xiangzhou District, Zhuhai 519070, China

* Correspondence: lihailiang@jnu.edu.cn; Tel.: +86-0756-8505761

Abstract: The application of batteries has become more and more extensive, and the heat dissipation problem cannot be ignored. Oscillating Heat Pipe (OHP) is a good means of heat dissipation. In this paper, the methods to improve the energy conversion and flow thermal performance of micro-channel OHP are studied and summarized. The working principle, heat transfer mechanism, advantages and applications of PHP are also introduced in detail in this study. Proper adjustment of the micro-channel layout can increase the heat transfer limit of PHP by 44%. The thermal resistance of two-diameter channel PHP is 45% lower than that of conventional PHP. The thermal resistance of PHP under uneven heating can be reduced to 50% of the original. PHP pulse heating can alleviate the phenomenon of dryness. Different working fluids have different effects on PHP. The use of graphene nano-fluids as the work medium can reduce the thermal resistance of PHP by 83.6%. The work medium obtained by the mixture of different fluids has the potential to compensate for the defects while inheriting the advantages of a single fluid.

Keywords: battery dissipation; energy conversion; oscillating heat pipe; thermal resistance; work medium



Citation: Zhao, X.; Zhu, Y.; Li, H. Micro-Channel Oscillating Heat Pipe Energy Conversion Approach of Battery Heat Dissipation Improvement: A Review. *Energies* **2022**, *15*, 7391. <https://doi.org/10.3390/en15197391>

Academic Editor: Gabriela Humnic

Received: 5 September 2022

Accepted: 29 September 2022

Published: 9 October 2022

Publisher's Note: MDPI stays neutral with regard to jurisdictional claims in published maps and institutional affiliations.



Copyright: © 2022 by the authors. Licensee MDPI, Basel, Switzerland. This article is an open access article distributed under the terms and conditions of the Creative Commons Attribution (CC BY) license (<https://creativecommons.org/licenses/by/4.0/>).

1. Introduction

The efficient and stable transfer of heat is the basis for the safe operation of batteries [1]. OHP were proposed by Akachi in 1990 [2,3], which is also named pulsating heat pipe (PHP). OHP has the advantages of high thermal efficiency, simple structure, easy miniaturization, high degree of customization, which are considered to have broad prospects in the fields of battery cooling, energy-saving transmission [4] and superconducting cooling [5]. When OHP works, the heat transfer of phase change is mainly carried out through the circulating flow of liquid plugs and steam plugs which randomly distributed in the pipeline [6]. The evaporation of the liquid film, the heat transferred and generated by the Taylor bubbles and flowing [7,8], which promotes the work fluid in the pipe flow. Micro-channel PHP consists of three parts: the evaporation section, the adiabatic section and the condensation section. The evaporation section is placed at the hot end to absorb heat. The condensation section is placed at the cold end to dissipate heat [9].

The structure of PHP is simple, but its mechanism in the process of heat and mass transfer is still in the exploratory stage [10,11]. PHP is generally studied by the simulation of the work fluid flow in the tube [12] or by an experiment [13,14]. The research on PHP mainly focuses on the heating conditions [15], the PHP structure [16,17], the effect of work fluid on the properties of PHP [18,19] and the flow [20]. The work fluid has a great influence on the thermal performance of PHP. The nano-fluids have become a research hotspot in recent years due to their excellent physical properties and the ability to enhance the performance of PHP.

The heat transfer function of the micro-channel PHP is mainly completed by heat convection and heat conduction. Geometry changes the flow of the work medium and the conduction path of the heat, which will affect the energy conversion of the micro-channel

PHP. Xie F et al. [21] observed that the average heat transfer coefficient of closed loop pulsating heat pipe (CLPHP) using a right-angle elbow in the evaporation section reached $1477 \text{ W}/(\text{m}^2 \cdot \text{K})$, which was higher than that of the CLPHP (circular evaporation section). The heat transfer of CLPHP under multi-source heat input stability has been significantly improved. Pagliarini et al. [22] studied a 3D closed-loop heat pipe using methanol as the work fluid. The layout is less affected by gravity than the plane layout at high input power and the equivalent thermal resistance can reach $0.25 \text{ K}/\text{W}$. The performance of 3D flat-plate oscillating heat pipe (FP-OHP) with staggered micro-channels was investigated by Thompson et al. [23]. The thermal resistance of 3D FP-OHP was as low as $0.08 \text{ }^\circ\text{C}/\text{W}$. The temperature change caused by the increase in wall temperature in the evaporation section under local heating increase.

High-speed camera visualization [24] and infrared analysis [25] were used to observe the flow characteristics. Heat transfer behavior of PHP in experiments, which can obtain an accurate understanding of the operation of PHP. The heat transfer performance of PHP is analyzed. The model is established by studying fluid dynamic phenomena and local heat flux density. Many researchers simulated the operation of PHP through the establishment of mathematical models [26,27] or mathematical methods to analyze the flow pattern of the work fluid inside of PHP [28]. Czajkowski et al. [29] studied the feasibility of U-shaped tube application by flow simulation based on the momentum and energy equations in the rotating coordinate system. Peng H et al. [30] proposed a fully nonlinear thermo-mechanical finite element model to simulate the oscillation of liquid plug, temperature distribution and heat transfer performance of PHP. The proposed thermodynamic model can accurately simulate PHP. In recent years, machine learning has been applied by researchers to predict the oscillatory motion, heat transfer of PHP due to its powerful information processing capability. Yoon A et al. [31] studied the oscillatory motion of liquid in PHP based on a deep neural network (DNN) model. The error was within 30% of predicting the average volume fraction of univariate and multivariate cases which provided an analysis of the fluid motion in PHP unique way of the situation. Qian N et al. [32] studied and predicted the heat transfer of PHP in the working process based on the extreme gradient boosting algorithm. The average absolute error was as low as 0.01%, which is expected to provide guidance for PHP studies.

Micro-channel OHP are widely applied which is important for improving the energy conversion pathway. This paper discusses the methods to improve the energy conversion of the micro-channel OHP. The work principle, heat transfer mechanism, advantages and applications of PHP are introduced in detail. The energy conversion methods and technologies are introduced, which involve physical structure of section, number of turns, valves, fins, material properties, heat source and pressure fluctuations. The research results can provide a favorable technical reference for battery heat dissipation.

2. Work Principle, Advantages and Applications

The structure of the micro-channel PHP is simple. The mechanism is complex and the running process is transient. Multiple stage changes occur in a short period of time of heat generation, flow heat transfer and efficient heat dissipation, etc. [33].

2.1. Work Principle and Heat Transfer Mechanism

The micro-channel PHP is usually formed by bending a capillary tube with a small inner diameter, which is generally serpentine or continuous U-shaped. After the tube is filled with work medium, it is evacuated [34] and sealed. Heat is transferred from the evaporation section to the condensation section by an oscillating two-phase flow [35]. Under the action of surface tension and temperature difference between the two ends [36], the work fluid in the tube forms bubbles and randomly distributed vapor and liquid plugs [37]. The liquid plug and liquid film in the evaporation section evaporate continuously after heat, which leads to the expansion of the bubbles. The steam plug increases the pressure in the evaporation section. Under the action of the pressure difference between the two

ends, the work medium is pushed to the condensation section which can release heat in the condensation section. The air pressure decreases after the condensation section is cooled and condensed. The bubbles and the steam plug condense and flow into the evaporation section under the action of gravity [38]. The residual steam and liquid plugs flow into the next condensation section through the turn, which can form a stable circulation without additional input power to drive. The working process of PHP is listed in Figure 1.

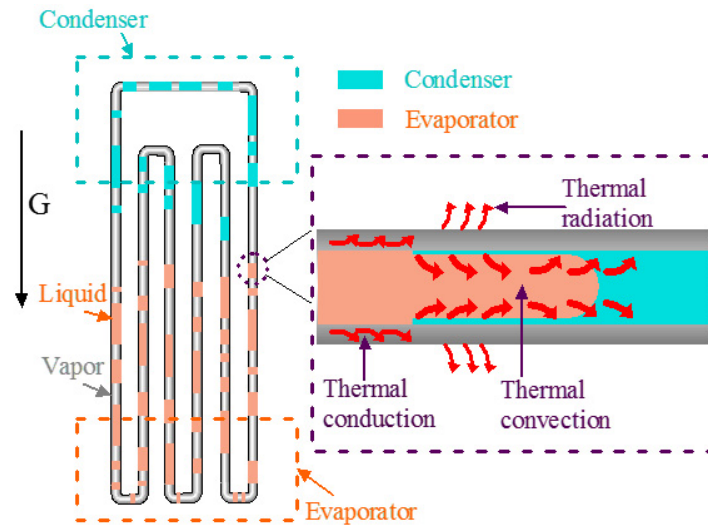


Figure 1. The working process of PHP. (The orange colour is the bubbles in evaporation section. The light blue colour is the bubbles in condenser section. The red colour is heat transmission).

The heat transfer methods include convection heat transfer, phase change latent heat transfer, etc. The factors of pressure difference, friction, inertial force, capillary force and gravity play an important role in coupling [39]. At the same time, the heat conduction of the tube wall cannot be ignored [40]. The initial distribution of the work fluid in the tube is not uniform. The vapor and liquid plugs appear at random positions, which lead to different pressure distributions in various parts of the tube, which cause random oscillation of the work fluid in the tube.

2.1.1. Thermal Convection of the PHP

During the operation of the micro-channel PHP, the pressure difference between the evaporation section and the condensation section pushes the work medium to the condensation section. The work medium flows back to the evaporation section after condensation. There is convective heat transfer in this process. Heat exchange of liquid convection is the main heat transfer mode in the PHP. The convective heat transfer coefficient of the two-phase flow in the vertical pipeline is given in Equations (1) and (2) [41]. The latent heat of the phase transition is given in Equation (3) [42].

$$h_{w-f} = h_l \left\{ 1 + 3000B_o^{0.86} + \left[\frac{x}{1-x} \right]^{0.75} \left(\frac{\rho_l}{\rho_v} \right)^{0.41} \right\} \quad (1)$$

$$h_{f-w} = h_l \left[(1-x)^{0.8} + \frac{3.8x^{0.76}(1-x)^{0.04}}{\left(\frac{P}{P_{cr}} \right)} \right] \quad (2)$$

$$h_{e,lat} \approx h_{c,lat} = \left(\frac{1 + 3.35Ca^{2/3}}{0.67Ca^{2/3}} \right) \frac{k_l}{D_h} \sim O(10^3) \quad (3)$$

where h_{w-f} and h_{f-w} are the heat transfer coefficients of convective boiling and convective cooling, $W/(m^2 \cdot K)$. k_l is the thermal conductivity of the liquid, $W/(m \cdot ^\circ C)$. h_l is the single-

phase heat transfer coefficient, $W/(m^2 \cdot K)$. q_{in} is heat flow, J/s . P is perimeter, m . P_{cr} is the perimeter of the section, m . B_o is the boiling number. x is the vapor mass of the evaporation section, kg . ρ_l and ρ_v are the liquid density and vapor density of the fluid, kg/m^3 . Ca is the capillary number of the micro-channel. D_h is the hydraulic diameter of the micro-channel, m . $h_{c,la}$ and $h_{c,lat}$ are the latent heat transfer coefficient of the condensation section of the evaporation section, $W/(m^2 \cdot K)$.

The flow of the work fluid inside the PHP will cause the heat conduction rate along the inner wall to be out of sync with the heat convection rate. The temperature gradient along the wall is greater than the temperature gradient along the fluid, which will result in convective heat transfer between the fluid and the wall [43]. The local convective heat flux density q between the fluid and the inner wall is shown in Equation (4).

$$q = \frac{\left(\rho c_p \frac{\partial T}{\partial t} - k \frac{\partial^2 T}{\partial z^2}\right) \cdot (r_{ext}^2 - r_{int}^2) + \frac{(T - T_{env})}{R_{env}} \cdot 2r_{ext}}{2r_{int}} \quad (4)$$

where k is the thermal conductivity of the micro-channel. T_{env} is the ambient temperature, $^{\circ}C$. R_{env} is the thermal resistance between the channel and the environment, which is assumed to be equal to $0.1 (m^2 \cdot K)/W$. T is the temperature, K . r normalized cross-correlation function. c_p is the constant pressure specific heat capacity, $J/(kg \cdot K)$. z is the coordinate, m .

Fluid convection will influence the choice of materials and dimensions when the evaporation section is designed [44]. The use of convection cooling in the condensation section can increase the cooling rate. A higher cooling air flow rate leads to an increase in the convective heat transfer coefficient, which accelerates the cooling rate of the evaporation and condensation sections [45]. When the heat input increases to a certain value, the evaporation section is likely to be completely dried up, which leads the PHP to reach the heat transfer limit. The increase in cooling air flow rate can raise the heat transfer limit of the PHP.

2.1.2. Heat Conduction of PHP

The heat transfer performance of FP-OHP is weakened because the transverse heat conduction of adjacent channels reduces the temperature gradient for the self-excited oscillation of the work medium [46]. The heat transfer rate of the tube wall is listed in Equation (5) [47].

$$q_w = -k A_s \frac{dT}{dr} = 2\pi L k \frac{T_i - T_o}{\ln(r_o/r_i)} \quad (5)$$

where T_i is the average temperature at the beginning, $^{\circ}C$. T_o is the average temperature at the end, $^{\circ}C$. L is the length, m . A_s is the cross-sectional area, m^2 . k is the thermal conductivity of the material, $W/(m \cdot K)$. r_i is the inner radius, m . r_o is the outer radius, m .

Due to the presence of tube heat conduction, the work fluid within the PHP cannot enter a stable state without the generation of air bubbles. Although bubble generation may not be directly involved in the development of the first oscillations, it plays a crucial role in preventing the oscillations from stopping [48]. The pipe material and section have a great influence on PHP startup [49]. The heat diffusion equation of the liquid plug i in the pipe is given in Equation (6), q''_w is the heat flux density with the pipe wall as shown in Equation (7) [50].

$$\rho_l c_{p,l} a^2 \frac{\partial T_{l,i}}{\partial t} = \lambda_l a^2 \frac{\partial^2 T_{l,i}}{\partial X_i^2} + 4a q''_w \quad (6)$$

$$q''_w = \begin{cases} \frac{\lambda_l Nu}{a} (T_H - T_{l,i}) & \text{(Evaporator)} \\ 0 & \text{(Adiabatic section)} \\ \frac{\lambda_l Nu}{a} (T_L - T_{l,i}) & \text{(Condenser)} \end{cases} \quad (7)$$

where ρ_l is the density of the liquid plug i , kg/m^3 . $c_{p,l}$ is the specific heat capacity of the liquid plug i , $J/(kg \cdot K)$. λ_l is the thermal conductivity, $W/(m \cdot K)$. T_i is the temperature of the liquid plug i , K . Nu is the Nusselt number. T_H and T_L are the evaporator and condenser temperatures, K .

2.2. Typical Advantages of PHP

2.2.1. Simple Structure for Manufacture

PHP has significant advantages of high efficiency and energy saving, which has wide application potential. PHP does not require the assistance of wicks or other structures, which relies on self-excited two-phase flow to function properly. Figure 2 is the structure of PHP. Ji Y et al. [51] fabricated a polydimethylsiloxane (PDMS) PHP using an aluminum mold and a PDMS plate, which consisted of only 5 turns of interconnecting channels bonded to a PDMS plate. Zhao et al. [52] designed a copper closed loop pulsating heat pipe (CLPHP). A red copper tube is bent five times and weld. The CLPHP can be regarded as a copper tube that does not contain other structures except the bent structure. Wu et al. [53] designed and fabricated a PHP for cooling metal cutting tools with the temperature reduce by 5–15%. The PHP is a copper tube is repeatedly bent through hole of the tool to absorb the heat generated by the tool. There is only a curved structure in the tube. Mahajan et al. [54] used PHP for waste heat recovery of ventilation systems with the recovery power of 240 W. The traditional heat pipe heat exchanger for waste heat recovery has an internal wicking structure, sintered screen or coaxial groove. The PHP is made by bending and welding a single copper pipe and the structure is relatively simple. Zhao et al. [55] used copper tube PHP with expanded graphite/graphite as the work fluid for thermal energy storage, which improved the safety of thermal management of power electronic equipment. The pipe body of PHP is made of bent and welded copper pipes. Alizadeh et al. [56] conducted a numerical simulation of a single-turn CLPHP for cooling photovoltaic modules. The use of PHP can increase the power generation of photovoltaic panels by about 18%. The single-turn CLPHP is an end-to-end quartz glass tube with a liquid-filled hole which has no additional complicated structure.

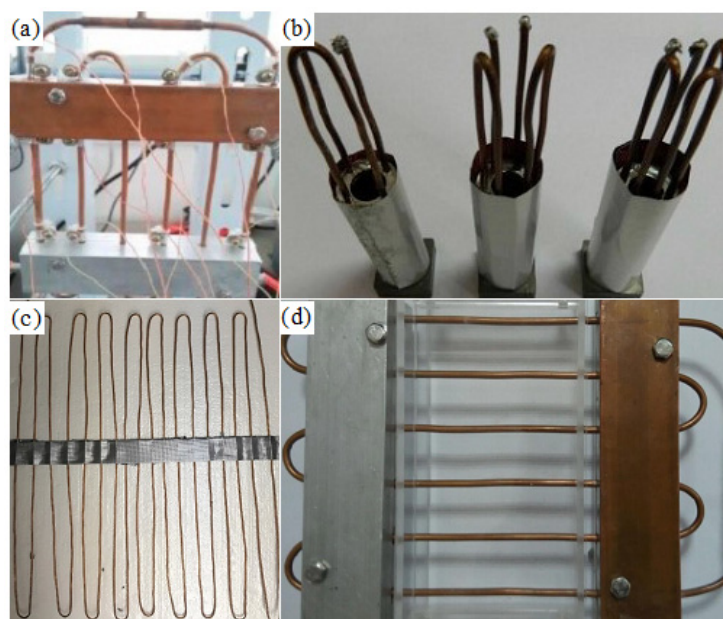


Figure 2. The structure of PHP: (a) The CLPHP [52]. Zhao et al. (2016); (b) The PHP for cooling metal cutting tools [53]. Wu et al. (2016); (c) The PHP for waste heat recovery [54]. Mahajan et al. (2018); (d) Copper tube PHP with expanded graphite/graphite [55]. Zhao et al. (2016).

2.2.2. Energy Saving with Excellent Heat Transfer Performance

PHP has excellent heat transfer performance, and it can be used as a heat exchanger in a heat recovery system or a solar collector system to save energy. Figure 3 is the experimental setup for AGPHP heat recovery. The use of PHP heat exchangers in air conditioning systems can reduce energy consumption to 14% [57]. Liu et al. [58] applied anti-gravity PHP to waste heat recovery. The test results showed that the heat recovery efficiency of anti-gravity PHP (AGPHP) was more than 1.66 times that of pure copper rods.

Deng et al. [59] tested a high-temperature exhaust waste heat recovery device based on anti-gravity PHP. The experimental device is displayed in Figure 4. The measured heat absorbed by AGPHP is 228% of pure copper meandering strips. The heat recovery efficiency is much better than traditional copper dielectric. Monroe et al. [60] achieved power generation while transferring heat through magnets. The coils connected in series with the PHP work medium. The maximum and average power generation at the heat input of 200 W were 428 μ W and 15.3 μ W, respectively. In remote areas without power coverage, the region has broad development potential. Li et al. [61] studied the graphene/water-ethylene glycol nano-suspension PHP for low temperature heat recovery. The measured minimum thermal resistance was 0.36 K/W, which can effectively improve the recovery efficiency of the low temperature heat recovery system. Khodami et al. [62] designed a PHP-based waste heat recovery device to recover waste heat from stack exhaust gas. The energy conversion rate was up to 22% in the test. Xu et al. [63] integrated PHP into a solar collector for heat transfer and the measured thermal resistance was as low as 0.26 $^{\circ}$ C/W. The thermal efficiency of the PHP-integrated solar collector was as high as 50%.

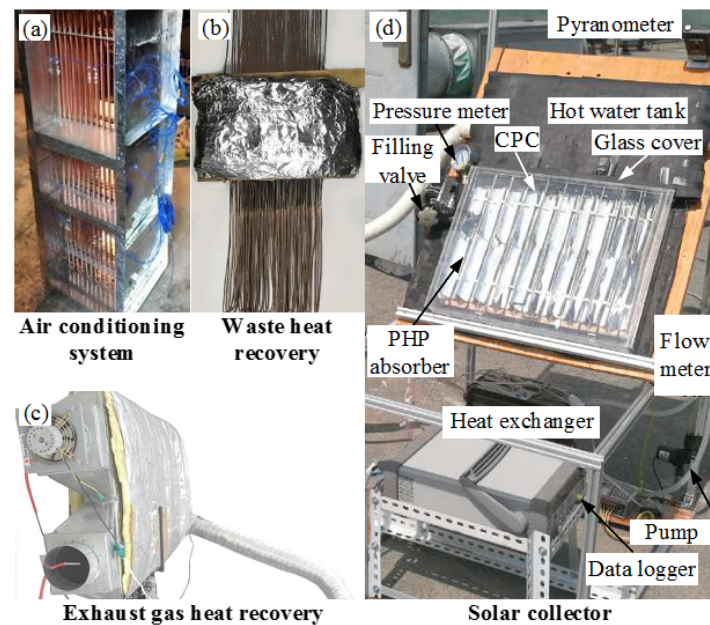


Figure 3. AGPHP heat recovery experiment: (a) Air conditioning system [57]. Barrak et al. (2020); (b) Waste heat recovery [58]. Liu et al. (2020); (c) Exhaust gas heat recovery [62]. Khodami et al. (2016); (d) Solar collector [63]. Xu et al. (2017).

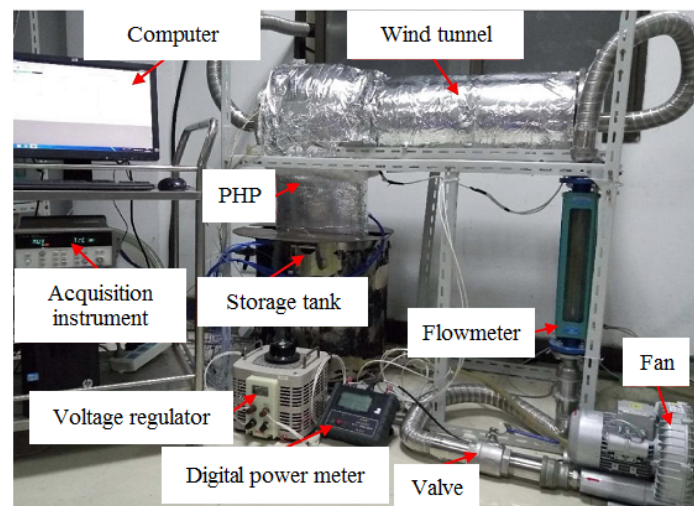


Figure 4. AGPHP heat recovery experiment [59]. Deng et al. (2017).

2.2.3. High Efficiency for Heat Dissipation

PHP can be used to cool and dissipate objects with high heat flux density of electronic components to ensure a safe temperature range. Experiments show that the heat transfer coefficient of multi-walled carbon nanotube nano-fluid PHP is 130% compared with conventional copper fins [64]. The thermal resistance of PHP at 800 rpm is $0.925\text{ }^{\circ}\text{C}/\text{W}$ [65] when it was applied to rotating equipment cooling. Czajkowski et al. [66] measured the thermal resistance of the rotating flower-shaped PHP. It decreased to $0.012\text{ }^{\circ}\text{C}/\text{W}$ with the increase in centrifugal acceleration. The structure is given in Figure 5, and it has a good application prospect in the field of heat dissipation of high heat flux devices. Ji et al. [67] fabricated and tested the high-temperature liquid metal PHP with the use of the sodium-potassium alloy as the work fluid. The thermal resistance of the high-temperature liquid metal PHP was at least $0.08\text{ }^{\circ}\text{C}/\text{W}$ at a working temperature above $500\text{ }^{\circ}\text{C}$. The low-temperature PHP of the cylindrical shell condenser studied by Sagar K R et al. [68] has an effective thermal conductivity of $16,350\text{ W}/(\text{m}\cdot\text{K})$ when the filling rate is 76%, which is about 32.7 times that of solid copper rods under the same conditions. Thompson et al. [69] tested multilayer Ti-6Al-4V-PHP fabricated with selective laser melting process. The effective thermal conductivity of multilayer Ti-6Al-4V-PHP was improved by 400% compared to solid Ti-6Al-4V-500%. Alizadeh et al. [70] conducted a numerical analysis of CLPHP heat dissipation of solar photovoltaic panels and found that the improvement rate of solar photovoltaic panels with CLPHP was 35.3%.

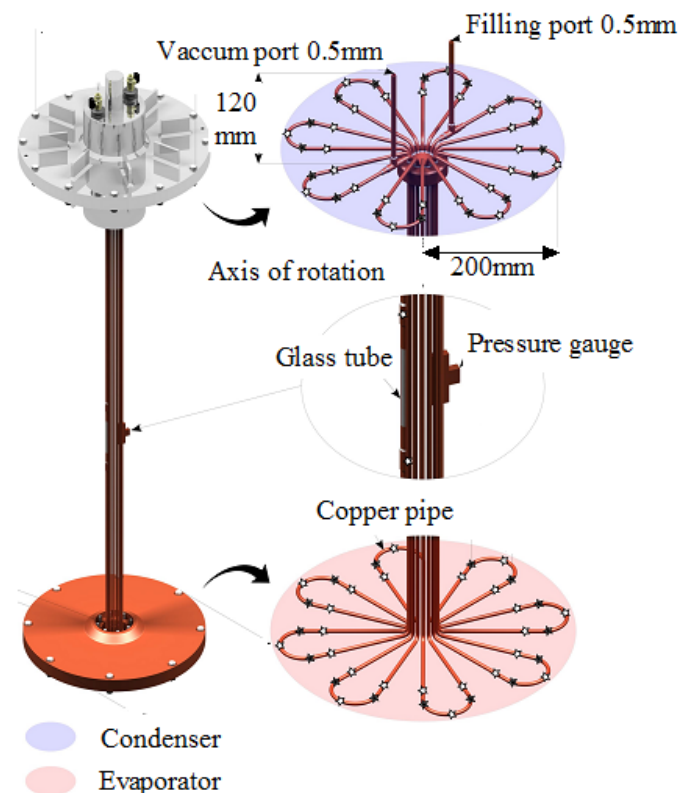


Figure 5. Rotating flower PHP [66]. Czajkowski et al. (2020).

2.3. Extensive Application and Promotion

Micro oscillation heat pipes (MPHP) can be fabricated by manufacture micro scale channels on silicon chips with microelectromechanical systems technology [71]. Liu [72] et al. tested the heat transfer performance of a silicon-based micro-oscillating heat pipe (MOHP) with the optimal filling rate of 53%. Dang et al. [73] carried out numerical simulation on the PHP cooling rack used to cool the central processing unit (CPU). The results showed that under the load of 1380 W, the CPU temperature of the PHP cooling rack was not more than $60\text{ }^{\circ}\text{C}$.

Figure 6 is the cooling arrangement of PHP. Qu et al. [74] measured the minimum thermal resistance of the silicon-based MPHP is $5.5\text{ }^{\circ}\text{C}/\text{W}$ and the startup time is less than 200 s. Kelly et al. [75] studied the radial PHP for the local heat dissipation of electronic equipment. The experiment of the radial PHP can reduce the temperature of the hotspot by $23\text{ }^{\circ}\text{C}$. Kearney et al. [76] studied the operation of embedded PHP of electronic equipment. The embedded PHP can operate normally under the heat flux density of at least $2.5\text{ W}/\text{cm}^2$. Jang et al. [77] tested the heat transfer performance of ultra-thin plate PHP of mobile electronic equipment. The thermal resistance of ultra-thin plate PHP at 90° and 0° with the inclination angles of 63% ($3\text{ }^{\circ}\text{C}/\text{W}$) and 56% ($3.6\text{ }^{\circ}\text{C}/\text{W}$), which is lower than that of graphite sheet.

Torresin et al. [78] tested a new type of PHP cooler. In the experiment, the influence of gravity is negligible. The lowest measured thermal resistance is $27\text{ K}/\text{kW}$. Qu et al. [79] studied the standard of PHP structure in the battery management system of new energy vehicles based on the flexible PHP made of a fluororubber tube. The heat transfer performance of PHP structures is in the order of “I” shape, “ladder” shape, “inverted U” shape and “N” shape. When the battery thermal management system is designed, the PHP can be selected according to the standard [80]. Chen et al. [81] tested the TiO_2 nano-fluid PHP of lithium iron phosphate battery thermal management. They measured the maximum temperature with the temperature gradient of the battery of $35.86\text{ }^{\circ}\text{C}$ and $1.15\text{ }^{\circ}\text{C}$. The improvement rate was 77% and the minimum thermal resistance was $0.098\text{ }^{\circ}\text{C}/\text{W}$. Ling et al. [82] proposed a cooling method for electronic devices which combined phase change material (PCM) with 3D PHP. The new cooling method can control the surface temperature of electronic devices below $100\text{ }^{\circ}\text{C}$, which is about $35\text{ }^{\circ}\text{C}$ lower than the air-cooling method with the thermal resistance reduce of 36.3% . Wang et al. [83] studied the 3D OHP for the photovoltaic cells cooling. The 3D OHP added with sintered copper particles in the evaporation section could keep the temperature of photovoltaic cells below $57\text{ }^{\circ}\text{C}$. Wang et al. [84] studied the thermal management system of lithium-ion power battery pack based on PCM/OHP. The maximum energy saving rate was 81.8% after using PCM/OHP battery management system. Wei et al. [85] tested plug-in PHP for the thermal management of electric vehicle batteries. Under the power input of 56 W , the minimum thermal resistance of PHP is $0.193\text{ }^{\circ}\text{C}/\text{W}$. The average temperature of the battery pack can be controlled below $46.5\text{ }^{\circ}\text{C}$ and the maximum temperature difference is $1\text{--}2\text{ }^{\circ}\text{C}$. Mosleh et al. [86] used PHP instead of fins in the air-cooled heat exchanger. The heat transfer coefficient of the air-cooled heat exchanger under natural convection forced convection were increased by 310% and 263% after using PHP instead of fins. Wang et al. [87] studied the application of PHP of LED heat dissipation based on PHP with sintered copper particles. The experimental setup is listed in Figure 7. Figure 7a is the LED heat sink, Figure 7b is the front side of LED chip and Figure 7c is the back side of PCB board. The addition of sintered copper particles is beneficial to the startup of PHP, since it can promote the oscillation movement. The maximum temperature of LED can be controlled below $70\text{ }^{\circ}\text{C}$.

Qian et al. [88] studied PHP for heat dissipation in the grinding wheel grinding area and showed that PHP can operate normally when the heat flux density is lower than $24,000\text{ W}/\text{m}^2$. The application of PHP in space had made great progress in recent years. Radiation PHP can be used for space applications requires an appropriate amount of heat input to start working at a lower operating temperature [89]. Iwata et al. [90] tested a metal flexible PHP of the spacecraft. The maximum thermal conductivity of the metal flexible PHP can reach $0.8\text{ W}/(\text{m}\cdot\text{K})$. The dynamic stiffnesses of the Y-axis and Z-axis are not more than $0.2\text{ N}/\text{mm}$, which is smaller than the graphite. Slobodeniuk et al. [91] designed a PHP composed of molybdenum and sapphire cover plate for the parabolic flight activities. Based on the We number and Ga number as defined in Equation (8), PHP was evaluated by the average We number obtained was the same as the reference critical value ($We_{crit} = 4$) and the Ga number (1980) was much higher than the reference critical value ($Ga_{crit} = 160$).

$$\begin{cases} We = \frac{\rho_l u^2 D_{crit}}{\sigma} \\ Ga = \left(\frac{(\rho_l - \rho_v) g D_{crit}^2}{\sigma} \right)^2 \frac{\rho_l u D_{crit}}{\mu_l} \end{cases} \quad (8)$$

where ρ_l , ρ_v , g , D_{crit} , σ , v , Re , μ_l are liquid, and vapor, densities, gravity acceleration, critical channel diameter, surface tension, liquid slug velocity, Reynolds number and liquid dynamic viscosity, respectively.

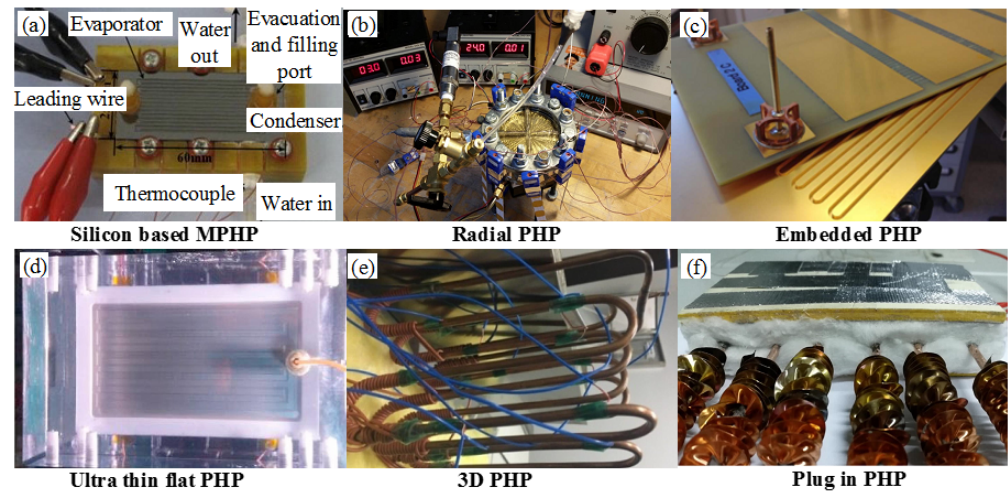


Figure 6. Cooling arrangement of PHP: (a) Silicon based MPHP [74]. Qu et al. (2012); (b) Radial PHP [75]. Kelly et al. (2018); (c) Embedded PHP [76]. Kearney et al. (2016); (d) Ultrathin flat PHP [77]. Jang et al. (2019); (e) 3D PHP [82]. Ling et al. (2020); (f) Plug in PHP [85]. Wei et al. (2019).

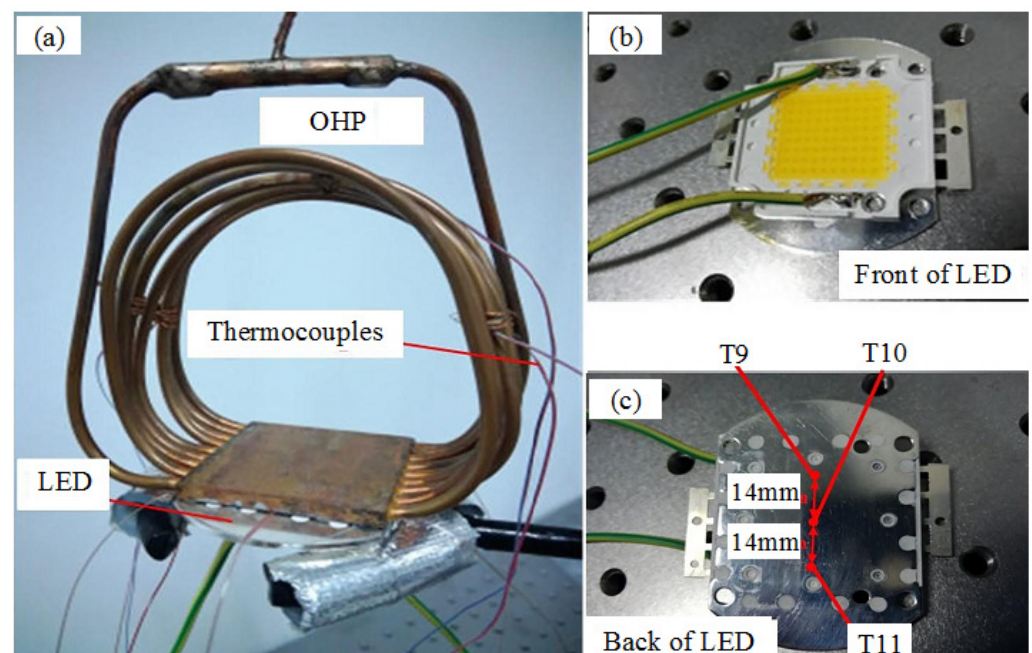


Figure 7. LED heat sink and PHP: (a) LED heat sink; (b) Front of LED chips; (c) Back of LED chips (T9, T10, and T11 are the LED backside temperatures obtained by three K-type thermocouples) [87]. Wang et al. (2019).

3. Methods for Improvement Energy Conversion of Micro-Channel PHP

Although the structure of micro-channel PHP is relatively simple, its heat and mass transfer mechanism are not clear. Its heat transfer performance is affected by many factors. The energy conversion efficiency improvement of micro-channel PHP is an important way to enhance the heat transfer performance of micro-channel PHP.

3.1. Influence of Section

When the inner diameter of the PHP section is too large, the surface tension of the work medium will decrease. The work medium tends to be layered by gravity which cannot work stably. When the inner diameter is too small, the work medium cannot overcome the oscillating flow resistance of the liquid plug between the cold and hot ends, which leads to the failure of start PHP [92]. Jiaqiang E et al. [93] proposed a new type of narrow tube closed PHP with retraction that can enhance the heat transfer performance of fixed direction oscillation cycle. The average heat transfer coefficient of the new narrow tube closed PHP was increased by 52.28% compared with that of the conventional PHP [94] and the average Prandel number (representing the ability of momentum diffusion and thermal fluid transfer) was increased by 25.49% compared with that of the conventional heat pipe. Hua C et al. [95] found the thermal resistance of rectangular channel PHP is only 30–40% of circular channel. The temperature difference between evaporation section and condensation section is 10–20 °C lower than that of circular channel PHP. Figure 8 is heat pipe structures with multiple elbows which are made from different materials. The variable diameter structure reduced the sensitivity of PHP to gravity and enhanced heat transfer performance by the pressure difference increase [96]. Tseng C Y et al. [97] studied the influence of alternate pipe diameters on the heat transfer performance of CLPHP based on CLPHP with 2.4 mm pipe diameters. Table 1 is some studies on PHP cross-sectional forms.

Table 1. Effect of PHP cross section on performance.

PHP Species	Work Medium	Section Type	Influence of Section
MPHP [94]	FC-72	Square	The square channel MPHP can handle the maximum allowable heat flux at about 70% higher than the circular channel MPHP.
Rectangular channel PHP [95]	Deionized Water	Rectangle	The start heating power of rectangular channel PHP is 1.5–2 times that of circular channel PHP.
CLPHP with alternate pipe diameters [97]	Water, Methanol, HFE-7100	Alternate pipe Diameter	The thermal resistance of CLPHP with alternate pipe diameters is about 11.5–34.9% of that of CLPHP with uniform pipe diameters.

The thermal resistance and start power of CLPHP with alternate pipe diameters were lower than conventional CLPHP. MARKAL B [98,99] studied the influence of double section ratio on PHP based on tapered PHP with double section ratio. The thermal resistance of tapered PHP with double section ratio is reduced by 28.4% compared with conventional PHP, which is not easily affected by gravity. The internal pressure fluctuation caused by the unequal hydraulic diameters of adjacent pipes leads to the heat transfer performance of the asymmetric micro pulsation heat exchanger which is better than that of the symmetric micro pulsation heat exchanger. Micro-channel OHP in battery heat management system and electronic device cooling has remarkable potential applications as listed in Table 2.

Table 2. The heat transfer performance of PHP application.

PHP Species	Work Medium	Minimum Thermal Resistance/K·W ⁻¹	Fill Rates/%	Input Power/W
MPHP [73]	Pure acetone	5	40, 53, 58, 61, 64, 74	4–10
OLPH [77]	Novec 649 Novec 774	0.2	30–70	–
Double condenser PHP [80]	R245fa	0.027	40–75	750–2400
PHP with sintered copper particles [94]	Ethanol	0.145	30–60	0–100
PHP with sintered copper particles [97]	Ethanol	0.168	30–50	10–60
Single loop PHP [99]	Acetone	0.54	55	–

The minimum thermal resistance is 3.4 °C/W [100]. Kwon G H et al. [101,102] studied the flow and heat transfer characteristics of dual diameter channel PHP. The thermal resistance of dual diameter channel PHP is 45% lower than that of conventional PHP.

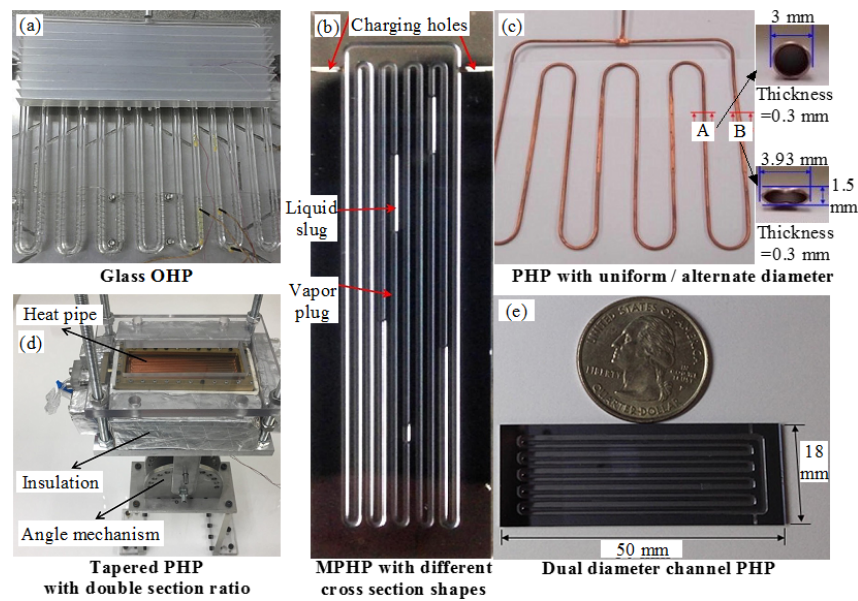


Figure 8. Heat pipe structure with multiple elbows: (a) Glass OHP [92]. Qu et al. (2016); (b) MPHP with different cross section shapes [94]. Lee and Kim, (2017); (c) PHP with uniform/alternate diameter [97]. Tseng et al. (2014); (d) Tapered PHP with double section ratio [98]. Markal et al. (2021); (e) Dual diameter channel PHP [102]. Kwon et al. (2015).

When the pressure difference generated by the channel diameter difference is greater than the friction pressure drop, the work medium can move without gravity as displayed in Figure 9. Figure 9a is the thermal conductivity greatly affected by gravity with dual diameter channels number of 1. Figure 9b is the thermal conductivity hardly affected by gravity with double diameter channels number of 3. Yang K S et al. [103] studied the flow characteristics of silicon-based MPHP pipes with different widths. The micro-channels with alternative widths introduce an unbalanced capillary force to promote the movement of vapor and liquid slugs. Tseng C Y et al. [104] proposed a new type of double pipe PHP. The thermal resistance of the new type of double pipe PHP can be as low as 0.0729 K/W.

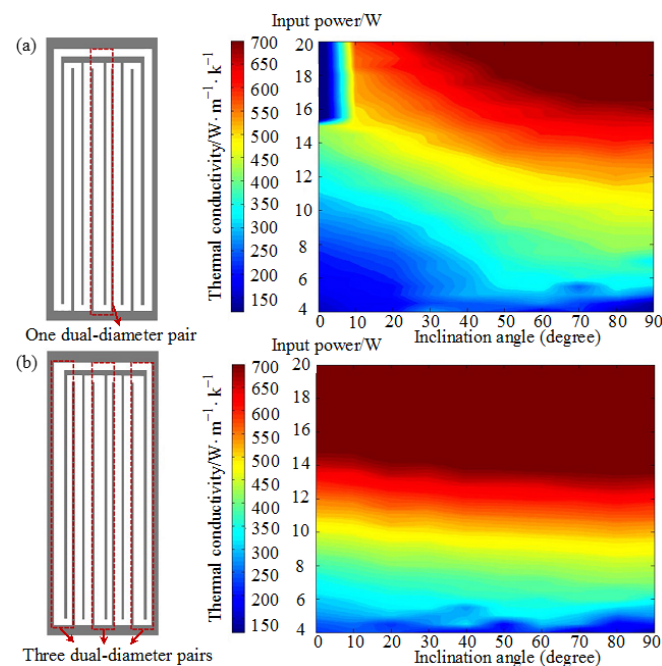


Figure 9. The thermal conductivity of MPHP affected by gravity: The MPHP has (a) one dual-diameter pair and (b) three dual-diameter pairs [102]. Kwon et al. (2015).

3.2. Characteristics of Turns

OHP turns lead to excessive flow resistance of the work medium in the pipe easily. When the turns number is too less, the oscillation of the work medium in the pipe is easier to stop. There is no recognized standard for the selection of PHP turns, which hinders the large-scale application of PHP [105]. Qian N et al. [106] described the startup process of single loop PHP through the second-order dynamic system control equation. The startup speed of single loop PHP depends on the type of work medium and heating power. Mameli M et al. [107] developed a numerical model for predicting the heat transfer performance of PHP. The flow reversal phenomenon caused 3 circles of CLPHP could not operate at the horizontal position and 9 circles of CLPHP could operate at the horizontal position. Spinato G et al. [108] found the thermal resistance of single circuit PHP reached the lowest value under high heat load and low filling rate. The film evaporation was the main local heat transfer mechanism. Lee et al. [109] studied the influence of turns on the heat transfer limit based on 5, 10, 15 and 20 turns of MPHP. The results are given in Figure 10. The influence of gravity on the maximum allowable heat flux of MPHP decreases with the increase in turns. Noh H Y et al. [110] studied the characteristics of 2 turns PHP and the heat transfer performance of PHP was affected by the mass flux of work medium. Kim B et al. [111] tested single loop, parallel and 2 turns PHP. Under low heating power, the thermal resistance of 2 turns PHP is smaller than that of parallel PHP. The influence of pressure drop is greater than the increase in disturbance under high heating power, which caused resistance of 2 turns PHP being larger than that of parallel PHP.

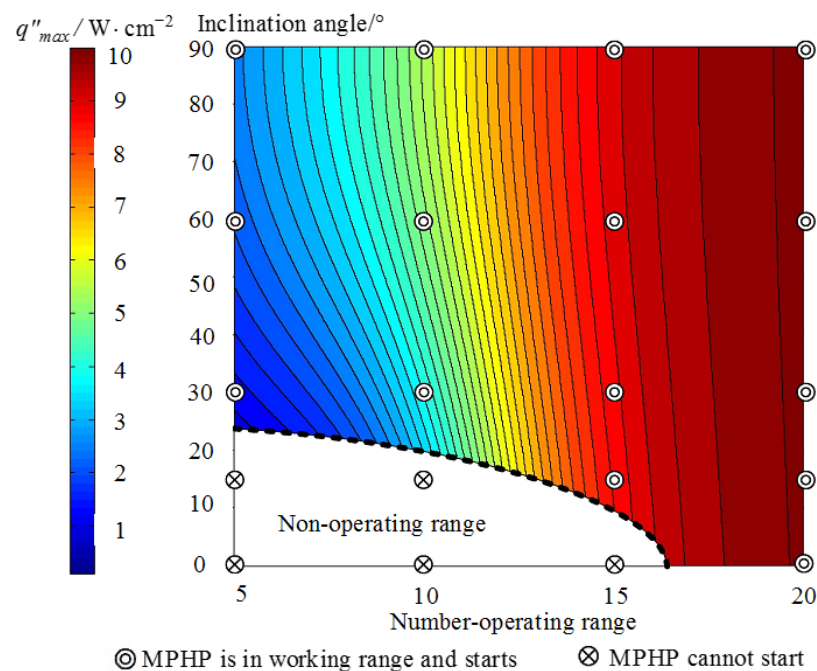


Figure 10. The maximum allowable heat flux density affected by gravity and turns number [109]. Lee et al. (2018).

3.3. Heat Transfer Performance Improvement of Pipeline Structure

Figure 11 is the pipeline structure of some PHPs. The pipeline structure of PHP affects the flow pattern and distribution of work fluid. Kim W et al. [112] compared the influence of cavity size on heat transfer performance based on the MPHP with cavity (10, 20, 30, 40 μm) and without cavity. The power required for startup of the MPHP with cavity was 50% lower than that without cavity. Kang Z et al. [113] studied a kind of PHP with partition walls based on numerical method. The heat transfer performance of PHP with partition walls can be improved by 14% compared with conventional PHP. The maximum equivalent thermal conductivity of PHP on the inner side of the partition wall is about

1194 W/(m·K). The maximum equivalent thermal conductivity is about 1977 W/(m·K) when the partition wall is located in the middle of the channel. Qu J et al. [114] studied the heat transfer performance under vertical heating based on micro groove PHP and the maximum effective thermal conductivity of PHP was 41.8 kW/(m·°C) at 40% filling rate. Lim J et al. [115] tested the influence of the channel arrangement on the plate MPHP under local heating. The amplitude oscillation of the liquid slug of the channel randomly arranged MPHP is larger than that of the channel with uniform channel arrangement, which makes it improve by 32% in heat transfer performance. Kim J et al. [116] and Wang J et al. [117] studied the influence of the length of evaporation section and condensation section on PHP.

As shown in Figure 12, the evaporation section is more likely to dry up with the increase in the length of condensation section. The heat exchange area of the MPHP improved with the increase in the length of the condensation section. The length ratio of the evaporation section increase in the condensation section will help CLPHP start and also reduce thermal resistance. Sedighi et al. [118,119] manufactured the additional branch PHP of a two-stage bubble pump in the evaporation section and compared the heat transfer performance of the additional branch PHP with that of the conventional FP-PHP. The bubble pump enhanced the flow cycle which resulted in less temperature fluctuation of the additional branch PHP. Kim et al. [120] carried out a visual study on the oscillatory motion of work medium in asymmetric MPHP. Two flow phenomena were oscillatory eruption mode (pressure periodic change) and circulation mode (the temperature rise in the evaporation section causes the expansion of the steam plug and the generation of circulation). Chiang C M et al. [121] established a model for predicting the asymmetric MPHP oscillation motion. The stronger oscillation motion caused by the larger average temperature difference between the evaporation section and the condensation section enhanced the heat transfer performance. Okazaki et al. [122] compared the conventional serpentine PHP with the closed-loop ring PHP. The thermal resistances are almost the same, which indicated that the design ideas of the PHP pipeline can be more diversified. Liu et al. [123] tested the heat transfer performance of the double serpentine channel flat plate OHP under multiple heat sources. The average equivalent thermal conductivity of the double serpentine channel flat plate OHP is 5.8 times than that of the pure 6063 aluminum alloy plate. The weight is only 83.6% of that of the pure 6063 aluminum alloy plate with the same geometry. Fonseca et al. [124] designed and tested a helium-based PHP, including 3 sub PHPs. The maximum effective thermal conductivity was 55,000 W/(m·K). Wang et al. [125] studied single loop PHP with a corrugated structure at different positions. The corrugated structure of evaporation section reduced the startup time by 28.96%. He et al. [126] promoted unidirectional flow in 3D CLPHP through series conical nozzles and the lower forward pressure drop alleviated the drying phenomenon with the lowest thermal resistance of 0.87 K/W.

Table 3 summarizes the improvement of heat transfer performance of OHP by some pipeline structures.

Table 3. Effect of OHP pipeline structure on performance.

PHP Species	Work Medium/Structure	Performance Improvement
MPHP with cavity [112]	Ethanol/With concave cavity	↓57% of thermal resistance
Micro slot PHP [114]	Water/Separation wall	The maximum allowable input heat flux is increased by 90 times
FPPHP [118,119]	Water/Secondary bubble pump	↓11–20% of thermal resistance
Double serpentine channel FPPHP [124]	Acetone/Double serpentine channel	The thermal conductivity is 5.8 times that of pure 6063 aluminum alloy plate, and it can be started at all inclination angles from 0° to 90°
Corrugated structure PHP [125]	Water/The evaporation section is of corrugated structure	Thermal resistance reduced by 37.57%
3D PHP [126]	Ethanol/Tandem conical nozzle	↓29.5% of thermal resistance

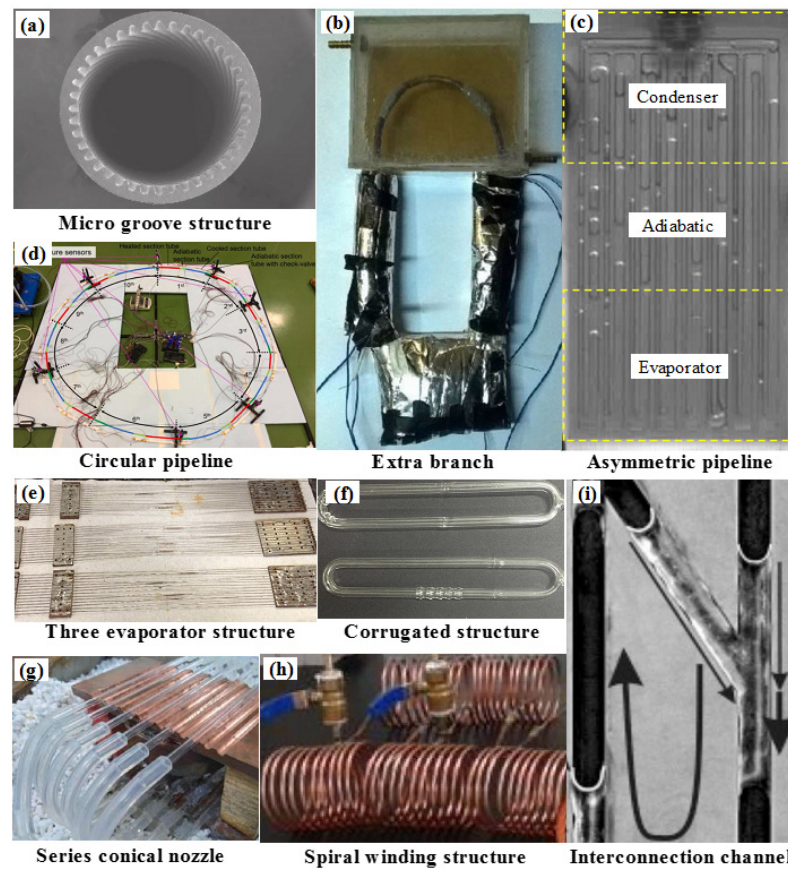


Figure 11. Partial pipeline structure: (a) Micro groove structure [114]. Qu et al. (2021); (b) Extra branch [119]. Sedighi et al. (2018). (c) Asymmetric pipeline [120]. Kim et al. (2018); (d) Circular pipeline [122]. Okazaki et al. (2021). (e) Three evaporator structure [124]. Fonseca et al. (2018); (f) Corrugated structure [125]. Wang et al. (2016); (g) Series conical nozzle [126]. He et al. (2020); (h) Spiral winding structure [127]. Yeboah et al. (2020); (i) Interconnection channel (the arrow indicates the flow direction of the liquid) [128]. Ebrahimi et al. (2015). (The arrow is the direction of movement. The dotted line is the regions of evaporator and condenser).

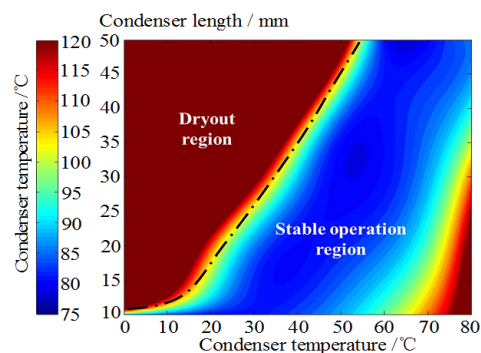


Figure 12. Temperature of condensation section and evaporation section under 18 W heating power [116]. Kim et al. (2018) (The dotted line is the dividing line of dryout region and stable operation region).

Yeboah et al. [127] designed an experiment for testing the copper spiral OHP with ethanol, methanol and deionized water as work fluids. Ebrahimi et al. [128] added interconnection channels in FP-PHP to enhance heat transfer and increased the working power range of FP-PHP. Qu et al. [129,130] studied 1–5 layers of 3D OHP and reported the thermal resistance of four layers of 3D OHP is the smallest when the heating power is less than 100 W. The copper tube with fewer layers of 3D OHP has less heat transfer and the

3D OHP with more layers has higher demand for heat input. The thermal resistance of two to five layers of 3D OHP is about $0.23\text{ }^{\circ}\text{C}/\text{W}$ when the heating power is 100 W . The 3-D OHP and 2-D OHP were compared with paraffin as the work medium as shown in Figure 13. Figure 13a is the structural diagram of 2D OHP and 3D OHP. Figure 13b is the schematic diagram of experimental equipment of four layers of 2-D OHP and 4 layers of 3D OHP. 1~8 are the positions of thermocouples. The melting time of wax in wax/3D OHP is longer during the heating process. The solidification time of wax/4-layer 2D-OHP and wax/4-layer 3D-OHP are about 0.48 and 0.29 times than that of pure wax, which indicated the heat transfer performance of PCM/3D OHP is better than PCM/OHP.

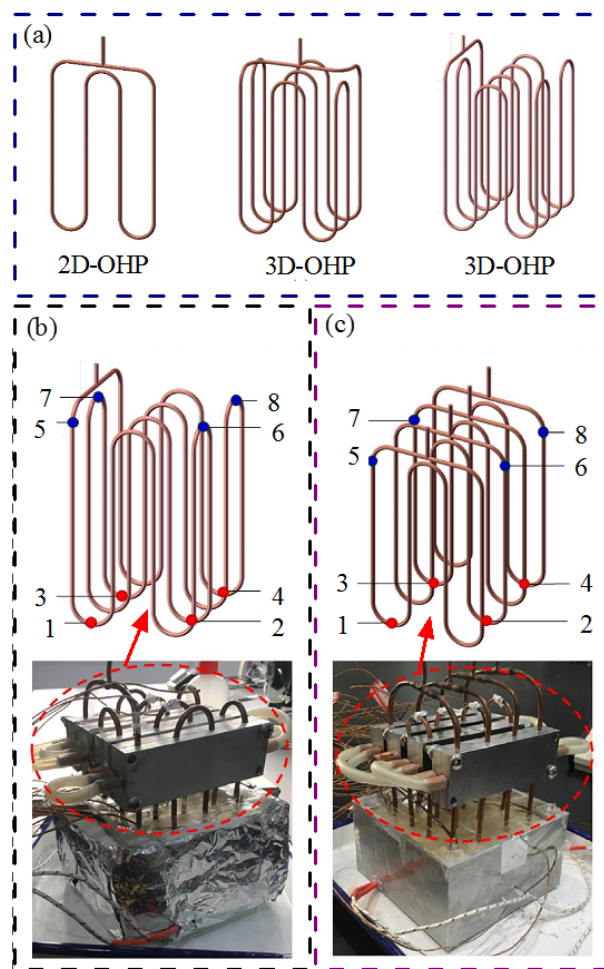


Figure 13. Schematic diagram of (a) 2D-OHP, 3 layers 3D-OHP and 4 layers 3D-OHP; Experimental system diagram of (b) 4 layers 3D-OHP and (c) 4 layers 2D-OHP, where 1~8 are the positions of thermocouples [130]. Qu et al. (2019). (The dotted circles is the test area).

3.4. Valves and Fins of the Work Medium

The use of valves helps PHP to promote and maintain the oscillation cycle of the work medium, which improved the heat transfer performance and stability. Ando et al. [131,132] investigated the effect of check valves on PHP start and heat transfer performance. The effective thermal conductivity of the check valve at normal weight is about $6000\text{ W}/(\text{m}\cdot\text{K})$, which is 30 times that of conventional aluminum alloy. The thermal resistance refers to no work fluid during the operation of PHP with a check valve and it can operate stably in space for 4 years. PHP enables stable start-up when the check valve is located near the condensation or insulation section. Fairley et al. [133] studied the effect of Tesla valves on PHP based on time-frequency analysis. The Tesla valves effectively reduced the occurrence of intermittent high-energy oscillations in the evaporation section of PHP by promoting circulating flow. De Vries et al. [134] found that Tesla valves reduced the

thermal resistance of PHP by about 14% by facilitating the circulation of the work fluid. Thompson et al. [135] observed the effect of Tesla valves on the internal flow of FP-PHP based on neutron radiography technology. The Tesla valves can make PHP by facilitating circulating flow. The thermal resistance is reduced by about 15 to 25%. Feng et al. [136] based on CLPHP with a spring-loaded check valve and studied the influence of the position of the check valve on the heat transfer performance. The experimental apparatuses are in Figure 14. The thermal resistance of CLPHP with a check valve is 25% lower than that of conventional CLPHP and the influence of gravity is weakened. Bhuwakietkumjohn et al. [137] discovered the flow pattern in PHP pipe with check valve changes from annular flow/segment plug flow to segment plug flow/bubble flow. Check valves, gravity and asymmetric heating all promote the flow cycle of the work medium. The synergy can enhance heat transfer when the promoters of loops move in opposite directions; the heat tolerance of PHP is enhanced [138]. Daimaru T et al. [139] simulated PHP with a check valve and observed that the localization of the liquid plug in the condensation section. The addition of fins helps to increase the heat transfer rate of PHP. Rahman et al. [140,141] studied the effect of fins on PHP. The use of fins in the condensation section can enhance the heat transfer effect significantly. Qu et al. [142] introduced micro fins in PHP, which reduced the thermal resistance by up to 41.7%. The effective thermal conductivity could reach 86,262 W/(m·K), which was about 216 times than that of large copper materials.

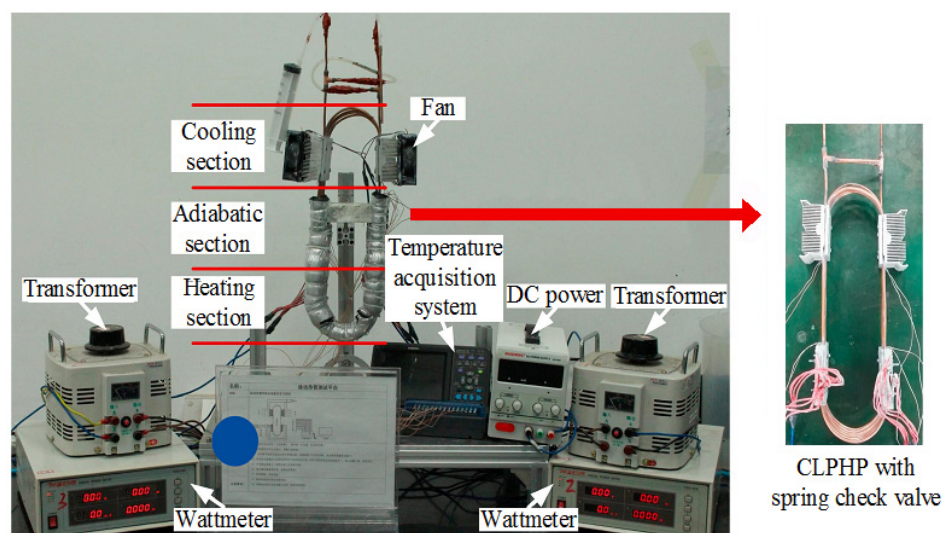


Figure 14. PHP with a spring-loaded check valve [136]. Feng et al. (2018).

3.5. Material Properties for Heat Transfer

The pipe body of PHP plays a certain role in the heat transfer. Odagiri et al. [143] established a 3D heat transfer model of aluminum flat PHP. The temperature difference in the thickness direction of aluminum PHP was relatively small (0.1 °C) through the simulation. The ratio of the maximum superheat of the hotspot to the average evaporation section temperature was between 9 and 11%. The equivalent thermal conductivity of polypropylene flat PHP is up to 6 times that of polypropylene sheets of the same size [144]. The effective thermal conductivity of polycarbonate PHP is up to 7000 W/(m·K) [145]. The residual sintered powder at the edge of Ti-6Al-4V PHP caused the work medium to produce core suction behavior. This suction behavior increases capillary pumping capacity, which reduced the PHP of gravity and start power [146]. Bhrumara [147] analyzed the heat transfer characteristics of copper PHP, which was consistent with experimental data. Lim J et al. [148] tested the heat transfer performance and stability of flexible OHP (FOHP) made of laminated film and low-density polyethylene. Figure 15 is flexible OHP (FOHP) when it is bended which is vertical under heating. The thermal resistance of FOHP is 2.41 K/W, which is 37% lower than that of copper OHP. The service life of FOHP is equivalent to 306 days in the standard atmosphere, which is 18 times that of conventional polymer OHP.

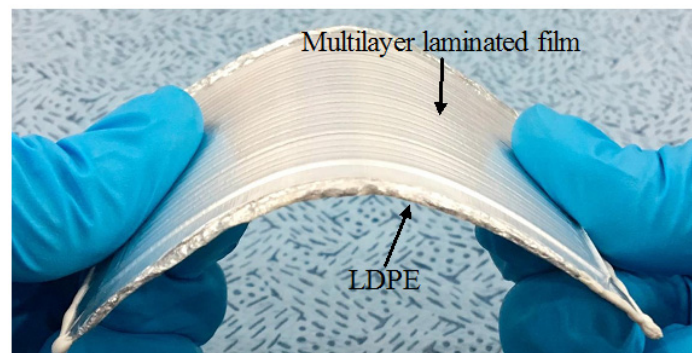


Figure 15. Flexible OHP [148]. Lim et al. (2018).

Qu et al. [149] tested the heat transfer properties of FOHP of different structures consisting of fluoroelastomer materials and micro-slot copper tubes. Figure 16a is the schematic diagram of different structures of FOHP. Figure 16b is the photographs of different structures of FOHP. The bending of the insulation section will lead to pressure loss. The start-up and heat transfer performance of FOHP is reduced and the heat transfer of FOHP performance is “i” shape, “step” shape, “inverted U” shape and “N” shape from high to low. PHP heat transfer performance can be improved by adjustment of the different wettability modes of the inner walls of the pipe [150]. Hao et al. [151] found the amplitude, velocity and liquid film length of the super-hydrophilic and hydrophilic pipe wall PHP were higher than those of copper PHP. The thermal resistance of the four-circle hydrophilic pipe wall PHP is reduced by about 5 to 15% and the thermal resistance of the six-circle super-hydrophilic and hydrophilic PHP is reduced by 5 to 15% and 15 to 25%, respectively. Betancur-Arboleda et al. [152] studied the effect of surface treatment on heat transfer properties of pipes based on copper PHP with different degrees of inner wall roughness. The thermal resistance of mixed sanding PHP (which uses standard sandpaper Grit N100 and Grit N1200 grinding in the evaporation section and the condensation section) is conventional 60% of PHP. Xie et al. [153] conducted chrome plating experiments on the inner wall of PHP aluminum tubes filled with moisture. which can reduce the thermal resistance of PHP to about 30% of the original. The stable working time was more than 5 times that of untreated PHP.

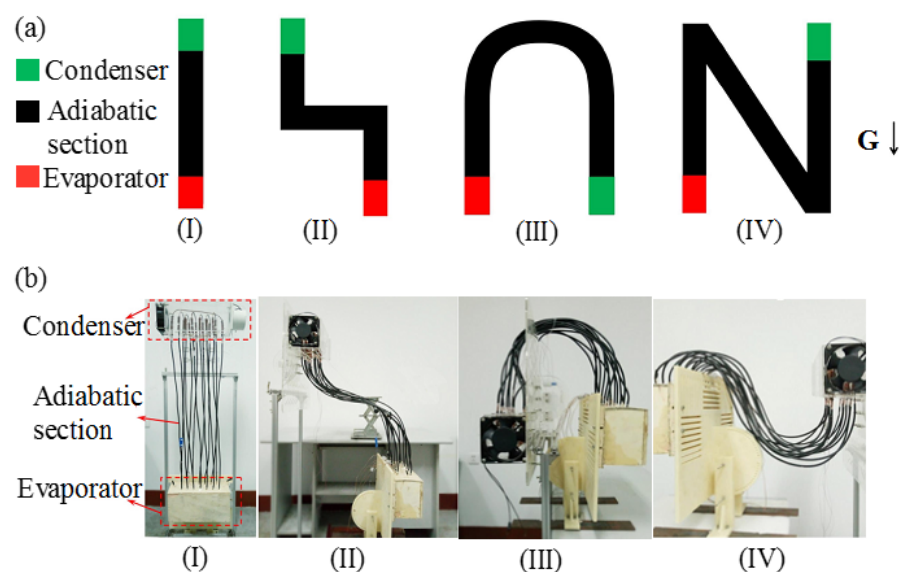


Figure 16. Schematic diagram (a) and photo (b) of FPHP with different flexible structures: (I) “I” shape, (II) “Ladder” shape, (III) “inverted-U” shape, and (IV) “N” shape [149]. Qu et al. (2017).

3.6. Heat Source Impact on the Temperature

In contrast to continuous heating, pulse heating can change its output power by constantly turning the heat source on and off. Taft B S et al. [154] found the input of PWM power does not affect the thermal resistance of PHP. The “injection-shrinkage” phenomenon of the work medium during pulse heating caused fluctuations in the pressure in the tube to enhance the heat transfer capacity [155]. In practice, PHP is susceptible to uneven heating. Mangini et al. [156] tested mixed PHP in uneven heating mode in space applications. The uneven heating can promote work medium circulation and improve the overall heat transfer performance. The thermal resistance of PHP is reduced by up to 8.7% under normal gravity. The excessive uneven heating tends to dry up the higher parts of the heating power. Jang D S et al. [157] used dimensionless thermal differences to express the degree of inhomogeneity as displayed in Equation (9).

$$\phi = \frac{Q_1 - Q_2}{Q_1 + Q_2} = \frac{Q_1 - Q_2}{Q_{total}} \quad (9)$$

where Q_1 and Q_2 are the heat inputs of two heat sources. Q_{total} is the total heat input. The thermal resistance and temperature difference increase with the increase in the dimensionless thermal difference.

Chen et al. [158] tested the heat transfer performance of series two-channel plate PHP under uneven heating and the experimental equipment which was shown in Figure 17. The heating of uneven PHP has better heat transfer performance at low heating power. The thermal resistance is about 15.3% of the same size pure 6063 aluminum alloy plate. When the heating power is higher, the heat transfer performance of the series two-channel flat plate PHP is even weaker than that of uniform heating. Zhao et al. [159] studied the work mass motion and heat transfer mechanism of PHP under different heating modes based on mathematical models. The heat transfer performance of PHP was increased by more than 6% under uneven heating. When the heating cycle under uniform pulse heating is short, the oscillation of the fluid maintains stable alternate heating and the dominant heat transfer is increased by 25%. Based on the topology optimization method, Lim et al. [160] proposed a channel layout design of plate MPHP under local heating. The experimental comparison results showed the design can reduce the thermal resistance of MPHP by 50%.

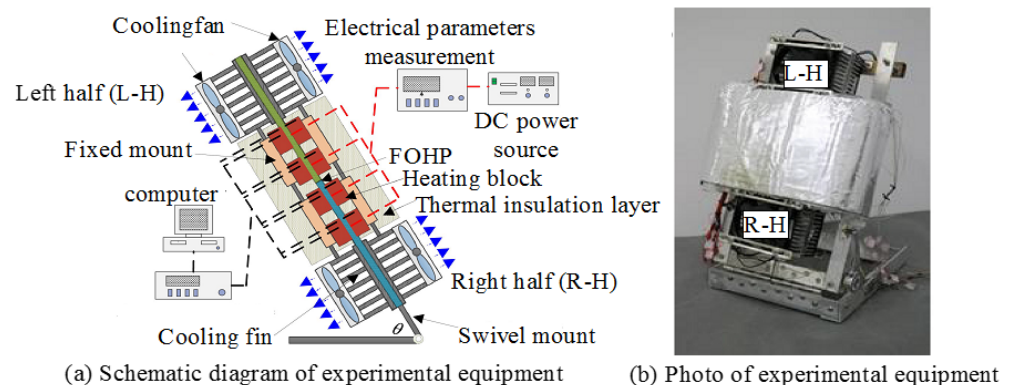


Figure 17. Schematic diagram (a) and photo (b) of a PHP device for a tandem tablet [158]. Chen et al. (2021).

3.7. Pressure Fluctuations of the PHP

The fluctuation in pressure in PHP is closely related to the generation of bubbles and liquid film. Pipe pressure affects the length of the steam plug and liquid plug, which leads to the heat transfer performance of PHP to change. Nine et al. [161] estimated the heat transfer performance of PHP by means of a pressure spectrum between the evaporation and condensation segments. The PHP had the lowest thermal resistance (about 0.25 °C/W) and the maximum pressure fluctuation at 2 wt% Cu/water nano-fluid as the work medium. Qu et al. [162] studied the effect of initial pressure on PHP with a thermal resistance increase of

493% at a heating power of 140 W, which was the initial pressure increased from 0.007 MPa to 0.065 MPa. The average temperature of the evaporation and condensation sections increased and decreased with the initial pressure improvement.

PHP fill rate affects fluctuations in pressure and the startup power increases as the fill rate improves [163]. Barua et al. [164] found the heat transfer performance of PHP depends on the work medium, filling rate and heating power. Fonseca et al. [165] studied the effect of filling rate on heat transfer performance based on low temperature PHP as given in Figure 18. The PHP has an effective thermal conductivity of 70,000 W/(m·K) at a filling rate of 20%. More heating power leads to more bubbles, which increased pressure fluctuations.

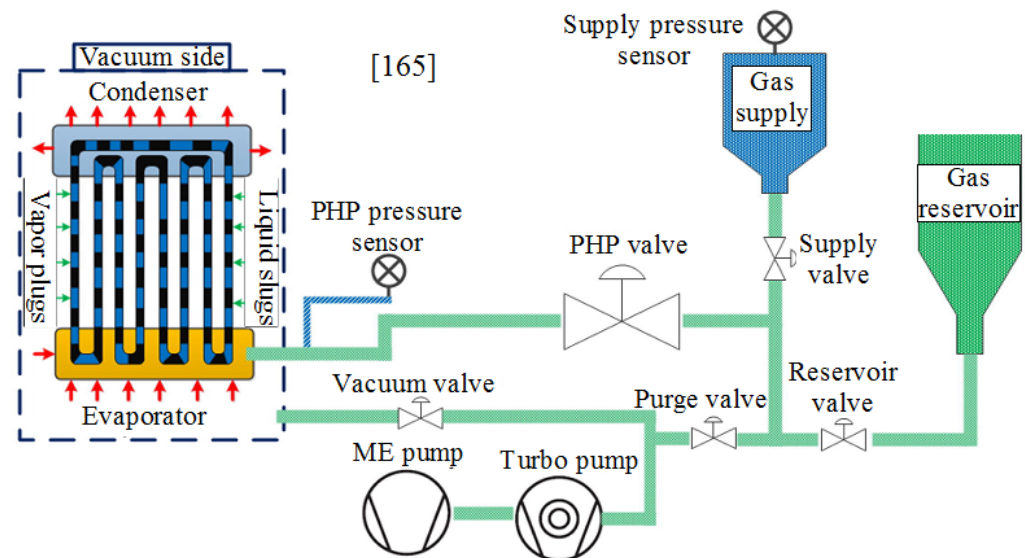


Figure 18. Low temperature PHP [165]. Fonseca et al. (2018).

4. Current Research Insufficient and Future Development Trends

4.1. Current Research Insufficient

- (1) The study of micro-channel layout mainly focuses on the thermal properties of PHP with a certain micro-channel layout design, which does not propose specific design specifications as a reference [166];
- (2) The study of pipeline structure is still in the stage of the pipeline geometry change and the heat transfer performance. The PHP heat transfer performance mechanism of pipeline structure is lacking in-depth description [167,168];
- (3) The study of materials and work fluids are not related to manufacturing and cost [169]. The work fluid is believed to be one of the factors that may have the greatest influence on PHP. Due to the complex hydrodynamic properties of the work medium, it is difficult to study the mechanism in the process of heat and mass transfer [170]. The certain kinds of work fluids of nano-fluids have own complex and properties which even under-fully recognized [171]. The stability of nano-fluids is a major problem of PHP applications [172];
- (4) The current research on PHP work fluids mainly focuses on the heat transfer performance or flow of PHP with a certain work medium [173]. The current research is lacking the selection criteria of the work medium under different conditions, which can only passively test the characteristics of the work fluid in experiments [174].

4.2. Future Trends

It can optimize the design of micro-channel layout for the future research trends of PHP. Appropriate adjustment of micro-channel layout can promote cyclic heat transfer [175]. Lee et al. [176] introduced a micro-stick array of the PHP micro-channel layout to increase the maximum permissible input power by 44%.

- (1) The prediction technology of PHP heat transfer performance is applied. Qian et al. [177] predicted the heat transfer performance of axial rotating OHP with an error of 3.36 to 16% with the grey system-based theory, which enhanced the heat transfer performance ability of PHP in industrial applications with only a small amount of data. Machine learning is applied to predict the heat transfer performance of PHP [178,179], which reduced the cost of PHP design, which is a reliable method for future PHP study;
- (2) Model optimization of PHP is studied. Chu et al. [180] proposed equations for the pressure difference and flow resistance of the work medium, which provided guidance for the structure optimization of PHP. Min et al. [181] introduced PHP in battery thermal management and compared the heat transfer performance of PHP with other cooling methods by modeling. Kang [182] et al. introduced porous core suction layers into PHP and established numerical models, which provided a new inspiration for the design of PHP;
- (3) A study trend focused on green environmental protection. In terms of environmental protection, it is a factor that must be taken into account in order to achieve sustainable development which reduced the carbon emissions and resources consumed with the PHP [183]. Monroe et al. [184] designed thermoelectric PHP with magnets and solenoids to recover waste heat into electrical energy, which is conducive to reducing carbon emissions and environmental pollution caused by power generation. PHP can also be combined with PCM materials which is applied to seawater desalination. It can save a lot of energy because it is a green and pollution-free seawater desalination technology [185,186];
- (4) The study of the relationship between the physical properties of the work fluid and the heat transfer properties of PHP can gain an in-depth understanding of the mechanism of PHP with the appropriate work medium [187]. Yasuda et al. [188] observed the flow of work fluids in PHP through neutron photography technology, which helped to explore the mechanism of work fluid flow. Wang J et al. [189] found the hydrophilicity of the pipe surface of numerical models, which can help to reduce the thermal resistance of CLPHP and improve the stability of the circulating flow;
- (5) Gravity PHP increases the drying limit of PHP by the reflux of the work fluid enhancement. PHP adaptability of the working environment will be improved [190]. Chen et al. [191] designed a tandem dual-channel FP-PHP for use in ultra-gravity environments, which can be applied to modern aerospace. Abela et al. [192] conducted experimental analysis and numerical simulation of PHP under microgravity. The prediction deviation was within 7%, which was helpful for studying the mechanism of gravity on PHP;
- (6) The exploration of industrial production is adopted. Low temperature PHP has the significant advantage of high thermal conductivity when it is used for superconductivity heat dissipation [193,194]. The application of PHP in industrial process will be explored [195];
- (7) The miniaturization of electronic equipment inevitably brings the problem of high heat flow density. The miniaturization of the heat dissipation system has become one of the mainstream directions of product iteration. The compact structure of PHP makes it easy to miniaturize and maintain good heat transfer performance. Silicon-based MPHP has micron-sized channels in which fluid flow and the heat transfer had some new characteristics compared to conventional capillary OHP [196]. Kamijima C et al. [197] measured $700 \text{ W}/(\text{m}\cdot\text{K})$ as the highest effective thermal conductivity of MPHP with a pipe diameter of $350 \mu\text{m}$. After miniaturization, PHP was able to work stably with excellent thermal performance. Lin et al. [198] studied the effective range of miniature oscillating heat pipes by experiment. Sun et al. [199] studied the working range of PHP after miniaturization. The MPHP can be started normally and operated stably. The effective fill rate of the horizontal direction is 40 to 55% when the vertical direction of the fill rate is 30 to 75%.

- (8) Heating applications are extended. PHP is usually used for heat dissipation due to its excellent heat transfer performance. The key step in the equation of the refrigeration and heating process is the heat transfer. PHP is well-used in refrigeration and heating. Aref L et al. [200] tested the thermal performance of flat-panel PHP solar collectors. The thermal efficiency reached 72.4% at a filling rate of 60% in sunny weather. Zhao J et al. [201] studied the heat transfer performance of solar with long-distance heat transmission PHP. The thermal resistance was as low as 0.0024 °C/W. Jin H et al. [202] used transparent PHP with nano-fluids as the work medium for the collection and transmission of solar energy. The maximum energy conversion efficiency can reach 92%. Zhao J et al. [203] conducted experimental tests on PHP-based large-scale heat storage systems. The use of self-humidifying fluids as work fluids would make PHP have greater heat transfer limits and longer heat transfer distances. Qu et al. [130,204] studied 3D PHP thermal properties for latent thermal energy storage (LHTES) devices. The efficiency of 3D OHP LHTES devices increased by about 32% compared to conventional devices and the heat storage was enhanced by PCM. Chen et al. [205] proposed ethane PHP based on stirling chillers. Xu et al. [206] designed PHP refrigeration equipment based on phase change energy storage technology and the utilization rate of PCM reached 78.7%. Saw L H et al. [207] designed a PHP-based roof cooling system which can reduce the temperature of the top floor of the house by 13%.

5. Conclusions

In this paper, the methods to improve the energy conversion and flow thermal performance of micro-channel PHP are studied. The use of appropriate physical structures can improve the heat transfer performance, start performance, operating range and stability of PHP. The work fluid is the main carrier of PHP heat transfer. The research and choice of the right work medium are key to achieving the desired performance of PHP.

- (1) The right structure and material choice had an important impact on PHP performance. Proper adjustment of the micro-channel layout can increase the heat transfer limit of PHP by 44%. The thermal resistance of 2D channel PHP is 45% lower than that of conventional PHP. The thermal resistance of FOHP can be as low as copper OHP of 63%;
- (2) In practical applications, different heating conditions of PHP are encountered. The thermal resistance of PHP under uneven heating can be reduced to 50% of the original. PHP pulse heating can alleviate the phenomenon of dryness;
- (3) Work fluids have different effects on PHP. The use of graphene nano-fluids as the work medium can reduce the thermal resistance of PHP by 83.6%. PHP with liquid nitrogen as the work medium can work at temperatures below 100 K. The work medium obtained by the mixture of different fluids has the potential to compensate for the defects while inheriting the advantages of a single fluid. The addition of self-humidifying nano-fluids to the graphene oxide nano-fluid can enhance the heat transfer performance of PHP by 12%, which can inhibit the drying phenomenon.

Author Contributions: X.Z.: Paper structure organization and writing, English writing and revision; Y.Z.: Paper search and drawing; H.L.: Data processing, English check. All authors have read and agreed to the published version of the manuscript.

Funding: This work was funded by the Young Scientists Fund of the National Natural Science Foundation of China, grant number 52106151. This work was funded by the Fundamental Research Funds for the Central Universities of 21621407.

Data Availability Statement: Not applicable.

Conflicts of Interest: The authors declare that they have no conflict of interests regarding the publication of this paper.

References

1. Akachi, H. Structure of A Heat Pipe. U.S. Patent 4,921,041, 1 May 1990.
2. Jun, S.; Kim, S.J. Comparison of the thermal performances and flow characteristics between closed-loop and closed-end micro pulsating heat pipes. *Int. J. Heat Mass Transf.* **2016**, *95*, 890–901. [[CrossRef](#)]
3. Kim, W.; Kim, S.J. Effect of a flow behavior on the thermal performance of closed-loop and closed-end pulsating heat pipes. *Int. J. Heat Mass Transf.* **2020**, *149*, 119251. [[CrossRef](#)]
4. Clement, J.; Wang, X. Experimental investigation of pulsating heat pipe performance with regard to fuel cell cooling application. *Appl. Therm. Eng.* **2013**, *50*, 268–274. [[CrossRef](#)]
5. Natsume, K.; Mito, T.; Yanagi, N.; Tamura, H.; Tamada, T.; Shikimachi, K.; Hirano, N.; Nagaya, S. Heat transfer performance of cryogenic oscillating heat pipes for effective cooling of superconducting magnets. *Cryogenics* **2011**, *51*, 309–314. [[CrossRef](#)]
6. Jo, J.; Kim, J.; Kim, S.J. Experimental investigations of heat transfer mechanisms of a pulsating heat pipe. *Energy Convers. Manag.* **2019**, *181*, 331–341. [[CrossRef](#)]
7. Mehta, B.; Khandekar, S. Taylor bubble-train flows and heat transfer in the context of pulsating heat pipes. *Int. J. Heat Mass Transf.* **2014**, *79*, 279–290. [[CrossRef](#)]
8. Pattamatta, A.; Sielaff, A.; Stephan, P. A numerical study on the hydrodynamic and heat transfer characteristics of oscillating Taylor bubble in a capillary tube. *Appl. Therm. Eng.* **2015**, *89*, 628–639. [[CrossRef](#)]
9. Ahmad, H.; Jung, S.Y. Effect of active and passive cooling on the thermo-hydrodynamic behaviors of the closed-loop pulsating heat pipes. *Int. J. Heat Mass Transf.* **2020**, *156*, 119814. [[CrossRef](#)]
10. Yoon, A.; Kim, S.J. Understanding of the thermo-hydrodynamic coupling in a micro pulsating heat pipe. *Int. J. Heat Mass Transf.* **2018**, *127*, 1004–1013. [[CrossRef](#)]
11. Jun, S.; Kim, S.J. Experimental investigation on the thermodynamic state of vapor plugs in pulsating heat pipes. *Int. J. Heat Mass Transf.* **2019**, *134*, 321–328. [[CrossRef](#)]
12. Wang, W.W.; Wang, L.; Cai, Y.; Yang, G.B.; Zhao, F.Y.; Liu, D.; Yu, Q.H. Thermo-hydrodynamic model and parametric optimization of a novel miniature closed oscillating heat pipe with periodic expansion-constriction condensers. *Int. J. Heat Mass Transf.* **2020**, *152*, 119460. [[CrossRef](#)]
13. Jung, C.; Lim, J.; Kim, S.J. Fabrication and evaluation of a high-performance flexible pulsating heat pipe hermetically sealed with metal. *Int. J. Heat Mass Transf.* **2020**, *149*, 119180. [[CrossRef](#)]
14. Liou, T.M.; Chang, S.W.; Cai, W.L.; Lan, I.A. Thermal fluid characteristics of pulsating heat pipe in radially rotating thin pad. *Int. J. Heat Mass Transf.* **2019**, *131*, 373–390. [[CrossRef](#)]
15. Shi, W.; Chen, H.; Pan, L.; Wang, Q. Start and running performance of a pulsating heat pipe with micro encapsulated phase change material. *Appl. Therm. Eng.* **2022**, *212*, 18626. [[CrossRef](#)]
16. Qu, J.; Sun, Q.; Wang, H.; Zhang, D.; Yuan, J. Performance characteristics of flat-plate oscillating heat pipe with porous metal-foam wicks. *Int. J. Heat Mass Transf.* **2019**, *137*, 30. [[CrossRef](#)]
17. Liu, J.; Shang, F.; Liu, D. Experimental study on enhanced heat transfer characteristics of synergistic coupling between the pulsating heat pipes. *Energy Procedia* **2012**, *16*, 1510–1516. [[CrossRef](#)]
18. Zhao, J.; Qu, J.; Rao, Z. Thermal characteristic and analysis of closed loop oscillation heat pipe/phase change material (CLOHP/PCM) coupling module with different working media. *Int. J. Heat Mass Transf.* **2018**, *126*, 257–266. [[CrossRef](#)]
19. Patel, V.M.; Mehta, H.B. Influence of working fluids on startup mechanism and thermal performance of a closed loop pulsating heat pipe. *Appl. Therm. Eng.* **2017**, *110*, 1568–1577. [[CrossRef](#)]
20. Hung, Y.H.; Teng, T.P.; Lin, B.G. Evaluation of the thermal performance of a heat pipe using alumina nanofluids. *Exp. Therm. Fluid Sci.* **2013**, *44*, 504–511. [[CrossRef](#)]
21. Xie, F.; Li, X.; Qian, P.; Huang, Z.; Liu, M. Effects of geometry and multisource heat input on flow and heat transfer in single closed-loop pulsating heat pipe. *Appl. Therm. Eng.* **2020**, *168*, 114856. [[CrossRef](#)]
22. Pagliarini, L.; Cattani, L.; Mameli, M.; Filippeschi, S.; Bozzoli, F.; Rainieri, S. Global and Local Heat Transfer Behaviour of a three-dimensional Pulsating Heat Pipe: Combined Effect of the Heat Load, Orientation and Condenser Temperature. *Appl. Therm. Eng.* **2021**, *195*, 17144. [[CrossRef](#)]
23. Thompson, S.M.; Cheng, P.; Ma, H.B. An experimental investigation of a three-dimensional flat-plate oscillating heat pipe with staggered microchannels. *Int. J. Heat Mass Transf.* **2011**, *54*, 3951–3959. [[CrossRef](#)]
24. Jun, S.; Kim, S.J. Experimental study on a criterion for normal operation of pulsating heat pipes in a horizontal orientation. *Int. J. Heat Mass Transf.* **2019**, *137*, 1064–1075. [[CrossRef](#)]
25. Cattani, L.; Mangini, D.; Bozzoli, F.; Pietrasanta, L.; Miche, N.; Mameli, M.; Filippeschi, S.; Rainieri, S.; Marengo, M. An original look into pulsating heat pipes: Inverse heat conduction approach for assessing the thermal behaviour. *Therm. Sci. Eng. Prog.* **2019**, *10*, 317–326. [[CrossRef](#)]
26. Lin, Z.; Wang, S.; Shirakashi, R.; Zhang, W. Simulation of a miniature oscillating heat pipe in bottom heating mode using CFD with unsteady modeling. *Int. J. Heat Mass Transf.* **2013**, *57*, 642–656. [[CrossRef](#)]
27. Manzoni, M.; Mameli, M.; De Falco, C.; Araneo, L.; Filippeschi, S.; Marengo, M. Non equilibrium lumped parameter model for Pulsating Heat Pipes: Validation in normal and hyper-gravity conditions. *Int. J. Heat Mass Transf.* **2016**, *97*, 473–485. [[CrossRef](#)]
28. Bhramara, P. CFD analysis of multi turn pulsating heat pipe. *Mater. Today Proc.* **2017**, *4*, 2701–2710.

29. Czajkowski, C.; Błasiak, P.; Rak, J.; Pietrowicz, S. The development and thermal analysis of a U-shaped pulsating tube operating in a rotating system of coordinates. *Int. J. Therm. Sci.* **2018**, *132*, 645–662. [[CrossRef](#)]
30. Peng, H.; Pai, P.F.; Ma, H. Nonlinear thermomechanical finite-element modeling, analysis and characterization of multi-turn oscillating heat pipes. *Int. J. Heat Mass Transf.* **2014**, *69*, 424–437. [[CrossRef](#)]
31. Yoon, A.; Kim, S.J. A deep-learning approach for predicting oscillating motion of liquid slugs in a closed-loop pulsating heat pipe. *Int. J. Heat Mass Transf.* **2021**, *181*, 121860. [[CrossRef](#)]
32. Qian, N.; Wang, X.; Fu, Y.; Zhao, Z.; Xu, J.; Chen, J. Predicting heat transfer of oscillating heat pipes for machining processes based on extreme gradient boosting algorithm. *Appl. Therm. Eng.* **2020**, *164*, 14521. [[CrossRef](#)]
33. Song, Y.; Xu, J. Chaotic behavior of pulsating heat pipes. *Int. J. Heat Mass Transf.* **2009**, *52*, 2932–2941. [[CrossRef](#)]
34. Nikolayev, V.S. Physical principles and state-of-the-art of modeling of the pulsating heat pipe: A review. *Appl. Therm. Eng.* **2021**, *195*, 17111. [[CrossRef](#)]
35. Kim, S.; Zhang, Y.; Choi, J. Effects of fluctuations of heating and cooling section temperatures on performance of a pulsating heat pipe. *Appl. Therm. Eng.* **2013**, *58*, 42–51. [[CrossRef](#)]
36. Sun, Q.; Qu, J.; Wang, Q.; Yuan, J. Operational characteristics of oscillating heat pipes under micro-gravity condition. *Int. Commun. Heat Mass Transf.* **2017**, *88*, 28–36. [[CrossRef](#)]
37. Senjaya, R.; Inoue, T. Bubble generation in oscillating heat pipe. *Appl. Therm. Eng.* **2013**, *60*, 251–255. [[CrossRef](#)]
38. Bastakoti, D.; Zhang, H.; Li, D.; Cai, W.; Li, F. An overview on the developing trend of pulsating heat pipe and its performance. *Appl. Therm. Eng.* **2018**, *141*, 305–332. [[CrossRef](#)]
39. Gürsel, G.; Frijns, A.J.H.; Homburg, F.G.A.; van Steenhoven, A. A mass-spring-damper model of a pulsating heat pipe with a non-uniform and asymmetric filling. *Appl. Therm. Eng.* **2015**, *91*, 90. [[CrossRef](#)]
40. Noh, H.Y.; Yoon, A.; Kim, S.J. Investigation into the effect of transverse conduction on the thermal performance of a flat-plate pulsating heat pipe. *Int. J. Heat Mass Transf.* **2021**, *181*, 121842. [[CrossRef](#)]
41. Singh, B.P.; Atrey, M.D. Numerical investigation of a nitrogen based cryogenic pulsating heat pipe. *Cryogenics* **2021**, *115*, 103246. [[CrossRef](#)]
42. Kim, J.; Kim, S.J. Experimental investigation on working fluid selection in a micro pulsating heat pipe. *Energy Convers. Manag.* **2020**, *205*, 112462. [[CrossRef](#)]
43. Monroe, J.G.; Aspin, Z.S.; Fairley, J.D.; Thompson, S.M. Analysis and comparison of internal and external temperature measurements of a tubular oscillating heat pipe. *Exp. Therm. Fluid Sci.* **2017**, *84*, 165–178. [[CrossRef](#)]
44. Goshayeshi, H.R.; Chaer, I. Experimental study and flow visualization of Fe₂O₃/kerosene in glass oscillating heat pipes. *Appl. Therm. Eng.* **2016**, *103*, 1213–1218. [[CrossRef](#)]
45. Zhou, Z.; Lv, Y.; Qu, J.; Sun, Q. DmitriiGrachev. Performance evaluation of hybrid oscillating heat pipe with carbon nanotube nanofluids for electric vehicle battery cooling. *Appl. Thermal. Eng.* **2021**, *196*, 117300. [[CrossRef](#)]
46. Takawale, A.; Abraham, S.; Sielaff, A.; Mahapatra, P.S.; Pattamatta, A.; Stephan, P. A comparative study of flow regimes and thermal performance between flat plate pulsating heat pipe and capillary tube pulsating heat pipe. *Appl. Therm. Eng.* **2019**, *149*, 613–624. [[CrossRef](#)]
47. Yeboah, S.K.; Darkwa, J. Thermal performance of a novel helically coiled oscillating heat pipe (HCOHP) for isothermal adsorption. an experimental study. *Int. J. Therm. Sci.* **2018**, *128*, 49–58. [[CrossRef](#)]
48. Nekrashevych, I.; Nikolayev, V.S. Effect of tube heat conduction on the pulsating heat pipe start-up. *Appl. Therm. Eng.* **2017**, *117*, 24–29. [[CrossRef](#)]
49. Nikolayev, V.S. Effect of tube heat conduction on the single branch pulsating heat pipe start-up. *Int. J. Heat Mass Transf.* **2016**, *95*, 477–487. [[CrossRef](#)]
50. Liang, Q.; Li, Y.; Wang, Q. Effects of filling ratio and condenser temperature on the thermal performance of a neon cryogenic oscillating heat pipe. *Cryogenics* **2018**, *89*, 102–106. [[CrossRef](#)]
51. Ji, Y.; Liu, G.; Ma, H.; Li, G.; Sun, Y. An experimental investigation of heat transfer performance in a polydimethylsiloxane (PDMS) oscillating heat pipe. *Appl. Therm. Eng.* **2013**, *61*, 690–697. [[CrossRef](#)]
52. Zhao, J.; Rao, Z.; Liu, C.; Li, Y. Experimental investigation on thermal performance of phase change material coupled with closed-loop oscillating heat pipe (PCM/CLOHP) used in thermal management. *Appl. Therm. Eng.* **2016**, *93*, 90–100. [[CrossRef](#)]
53. Wu, Z.; Yang, Y.; Luo, C. Design, fabrication and dry cutting performance of pulsating heat pipe self-cooling tools. *J. Clean. Prod.* **2016**, *124*, 276–282. [[CrossRef](#)]
54. Mahajan, G.; Thompson, S.M.; Cho, H. Experimental characterization of an n-pentane oscillating heat pipe for waste heat recovery in ventilation systems. *Heliyon* **2018**, *4*, e00922. [[CrossRef](#)]
55. Zhao, J.; Rao, Z.; Liu, C.; Li, Y. Experiment study of oscillating heat pipe and phase change materials coupled for thermal energy storage and thermal management. *Int. J. Heat Mass Transf.* **2016**, *99*, 252–260. [[CrossRef](#)]
56. Alizadeh, H.; Ghasempour, R.; Shafii, M.B.; Ahmadi, M.H.; Yan, W.M.; Alhuyi Nazari, M. Numerical simulation of PV cooling by using single turn pulsating heat pipe. *Int. J. Heat Mass Transf.* **2018**, *127*, 203–208. [[CrossRef](#)]
57. Barrak, A.S.; Saleh, A.A.M.; Naji, Z.H. An experimental study of using water, methanol, and binary fluids in oscillating heat pipe heat exchanger. *Eng. Sci. Technol. Int. J.* **2020**, *23*, 357–364. [[CrossRef](#)]
58. Liu, X.; Han, X.; Wang, Z.; Hao, G.; Zhang, Z.; Chen, Y. Application of an anti-gravity oscillating heat pipe on enhancement of waste heat recovery. *Energy Convers. Manag.* **2020**, *205*, 112404. [[CrossRef](#)]

59. Deng, Z.; Zheng, Y.; Liu, X.; Zhu, B.; Chen, Y. Experimental study on thermal performance of an anti-gravity pulsating heat pipe and its application on heat recovery utilization. *Appl. Therm. Eng.* **2017**, *125*, 1368–1378. [[CrossRef](#)]
60. Monroe, J.G.; Ibrahim, O.T.; Thompson, S.M.; Shamsaei, M. Energy harvesting via fluidic agitation of a magnet within an oscillating heat pipe. *Appl. Therm. Eng.* **2018**, *129*, 884–892. [[CrossRef](#)]
61. Li, Z.; Sarafraz, M.M.; Mazinani, A.; Moria, H.; Tlili, I.; Alkanhal, T.A.; Goodarzi, M.; Safaei, M.R. Operation analysis, response and performance evaluation of a pulsating heat pipe for low temperature heat recovery. *Energy Convers. Manag.* **2020**, *222*, 113230. [[CrossRef](#)]
62. Khodami, R.; Nejad, A.A.; Khabbaz, M.R.A. Experimental investigation of energy and exergy efficiency of a pulsating heat pipe for chimney heat recovery. *Sustain. Energy Technol. Assess.* **2016**, *16*, 11–17. [[CrossRef](#)]
63. Xu, R.J.; Zhang, X.H.; Wang, R.X.; Xu, S.H.; Wang, S.H. Experimental investigation of a solar collector integrated with a pulsating heat pipe and a compound parabolic concentrator. *Energy Convers. Manag.* **2017**, *148*, 68–77. [[CrossRef](#)]
64. Kazemi-Beydokhti, A.; Meyghani, N.; Samadi, M.; Hajiabadi, S.H. Surface modification of carbon nanotube: Effects on pulsating heat pipe heat transfer. *Chem. Eng. Res. Des.* **2019**, *152*, 30–37. [[CrossRef](#)]
65. Dehshali, M.E.; Nazari, M.A.; Shafii, M.B. Thermal performance of rotating closed-loop pulsating heat pipes: Experimental investigation and semi-empirical correlation. *Int. J. Therm. Sci.* **2018**, *123*, 14–26. [[CrossRef](#)]
66. Czajkowski, C.; Nowak, A.I.; Pietrowicz, S. Flower Shape Oscillating Heat Pipe—A novel type of oscillating heat pipe in a rotary system of coordinates—An experimental investigation. *Appl. Therm. Eng.* **2020**, *179*, 115702. [[CrossRef](#)]
67. Ji, Y.; Wu, M.; Feng, Y.; Yu, C.; Chu, L.; Chang, C.; Li, Y.; Xiao, X.; Ma, H. An experimental investigation on the heat transfer performance of a liquid metal high-temperature oscillating heat pipe. *Int. J. Heat Mass Transf.* **2020**, *149*, 119198. [[CrossRef](#)]
68. Sagar, K.R.; Desai, A.B.; Naik, H.B.; Mehta, H.B. Experimental investigations on two-turn cryogenic pulsating heat pipe with cylindrical shell-type condenser. *Appl. Therm. Eng.* **2021**, *196*, 117240. [[CrossRef](#)]
69. Thompson, S.M.; Aspin, Z.S.; Shamsaei, N.; Elwany, A.; Bian, L. Additive manufacturing of heat exchangers: A case study on a multi-layered Ti–6Al–4V oscillating heat pipe. *Addit. Manuf.* **2015**, *8*, 163–174. [[CrossRef](#)]
70. Alizadeh, H.; Nazari, M.A.; Ghasempour, R.; Shafii, M.B.; Akbarzadeh, A. Numerical analysis of photovoltaic solar panel cooling by a flat plate closed-loop pulsating heat pipe. *Sol. Energy* **2020**, *206*, 455–463. [[CrossRef](#)]
71. Ocaña, J.L.; Morales, M.; Molpeceres, C.; Garcia, O.; Porro, J.A.; Garcia-Ballesteros, J. Short pulse laser microforming of thin metal sheets for MEMS manufacturing. *Appl. Surf. Sci.* **2007**, *254*, 997–1001. [[CrossRef](#)]
72. Liu, X.; Xu, L.; Wang, C.; Han, X. Experimental study on thermo-hydrodynamic characteristics in a micro oscillating heat pipe. *Exp. Therm. Fluid Sci.* **2019**, *109*, 109871. [[CrossRef](#)]
73. Dang, C.; Jia, L.; Lu, Q. Investigation on thermal design of a rack with the pulsating heat pipe for cooling CPUs. *Appl. Therm. Eng.* **2017**, *110*, 390–398. [[CrossRef](#)]
74. Qu, J.; Wu, H.; Cheng, P. Start-up, heat transfer and flow characteristics of silicon-based micro pulsating heat pipes. *Int. J. Heat Mass Transf.* **2012**, *55*, 6109–6120. [[CrossRef](#)]
75. Kelly, B.; Hayashi, Y.; Kim, Y.J. Novel radial pulsating heat-pipe for high heat-flux thermal spreading. *Int. J. Heat Mass Transf.* **2018**, *121*, 97–106. [[CrossRef](#)]
76. Kearney, D.J.; Suleman, O.; Griffin, J.; Mavrakis, J. Thermal performance of a PCB embedded pulsating heat pipe for power electronics applications. *Appl. Therm. Eng.* **2016**, *98*, 798–809. [[CrossRef](#)]
77. Jang, D.S.; Kim, D.; Hong, S.H.; Kim, Y. Comparative thermal performance evaluation between ultrathin flat plate pulsating heat pipe and graphite sheet for mobile electronic devices at various operating conditions. *Appl. Therm. Eng.* **2019**, *149*, 1427–1434. [[CrossRef](#)]
78. Torresin, D.; Agostini, F.; Mularczyk, A.; Agostini, B.; Habert, M. Double condenser pulsating heat pipe cooler. *Appl. Therm. Eng.* **2017**, *126*, 1051–1057. [[CrossRef](#)]
79. Qu, J.; Wang, C.; Li, X.; Wang, H. Heat transfer performance of flexible oscillating heat pipes for electric/hybrid-electric vehicle battery thermal management. *Appl. Therm. Eng.* **2018**, *135*, 9. [[CrossRef](#)]
80. Rao, Z.; Huo, Y.; Liu, X. Experimental study of an OHP-cooled thermal management system for electric vehicle power battery. *Exp. Therm. Fluid Sci.* **2014**, *57*, 20–26. [[CrossRef](#)]
81. Chen, M.; Li, J. Nanofluid-based pulsating heat pipe for thermal management of lithium-ion batteries for electric vehicles. *J. Energy Storage* **2020**, *32*, 01715. [[CrossRef](#)]
82. Ling, Y.Z.; Zhang, X.S.; Wang, F.; She, X. Performance study of phase change materials coupled with three-dimensional oscillating heat pipes with different structures for electronic cooling. *Renew. Energy* **2020**, *154*, 636–649. [[CrossRef](#)]
83. Wang, H.; Qu, J.; Sun, Q.; Kang, Z.; Han, X. Thermal characteristic comparison of three-dimensional oscillating heat pipes with/without sintered copper particles inside flat-plate evaporator for concentrating photovoltaic cooling. *Appl. Therm. Eng.* **2020**, *167*, 114815. [[CrossRef](#)]
84. Wang, Q.; Rao, Z.; Huo, Y.; Wang, S. Thermal performance of phase change material/oscillating heat pipe-based battery thermal management system. *Int. J. Therm. Sci.* **2016**, *102*, 9–16. [[CrossRef](#)]
85. Wei, A.; Qu, J.; Qiu, H.; Wang, C.; Cao, G. Heat transfer characteristics of plug-in oscillating heat pipe with binary-fluid mixtures for electric vehicle battery thermal management. *Int. J. Heat Mass Transf.* **2019**, *135*, 746–760. [[CrossRef](#)]
86. Mosleh, H.J.; Bijarchi, M.A.; Shafii, M.B. Experimental and numerical investigation of using pulsating heat pipes instead of fins in air-cooled heat exchangers. *Energy Convers. Manag.* **2019**, *181*, 653–662. [[CrossRef](#)]

87. Wang, H.; Qu, J.; Peng, Y.; Sun, Q. Heat transfer performance of a novel tubular oscillating heat pipe with sintered copper particles inside flat-plate evaporator and high-power LED heat sink application. *Energy Convers. Manag.* **2019**, *189*, 215–222. [[CrossRef](#)]
88. Qian, N.; Fu, Y.; Zhang, Y.; Chen, J.; Xu, J. Experimental investigation of thermal performance of the oscillating heat pipe for the grinding wheel. *Int. J. Heat Mass Transf.* **2019**, *136*, 911–923. [[CrossRef](#)]
89. Pietrasanta, L.; Postorino, G.; Perna, R.; Mameli, M.; Filippeschi, S. A pulsating heat pipe embedded radiator: Thermal-vacuum characterisation in the pre-cryogenic temperature range for space applications. *Therm. Sci. Eng. Prog.* **2020**, *19*, 100622. [[CrossRef](#)]
90. Iwata, N.; Miyazaki, Y.; Yasuda, S.; Ogawa, H. Thermal performance and flexibility evaluation of metallic micro oscillating heat pipe for thermal strap. *Appl. Therm. Eng.* **2021**, *197*, 117342. [[CrossRef](#)]
91. Slobodeniuk, M.; Bertossi, R.; Ayel, V.; Ravichandran, R.; Thyagarajan, K.; Romestant, C.; Bertin, Y. Experimental study of the flat plate pulsating heat pipe operation during dry-out and flow re-activation periods under microgravity conditions. *Int. J. Multiph. Flow* **2021**, *147*, 103888. [[CrossRef](#)]
92. Qu, J.; Wang, Q.; Sun, Q. Lower limit of internal diameter for oscillating heat pipes: A theoretical model. *Int. J. Therm. Sci.* **2016**, *110*, 174–185. [[CrossRef](#)]
93. Jiaqiang, E.; Zhao, X.; Liu, H.; Chen, J.; Zuo, W.; Peng, Q. Field synergy analysis for enhancing heat transfer capability of a novel narrow-tube closed oscillating heat pipe. *Appl. Energy* **2016**, *175*, 218–228. [[CrossRef](#)]
94. Lee, J.; Kim, S.J. Effect of channel geometry on the operating limit of micro pulsating heat pipes. *Int. J. Heat Mass Transf.* **2017**, *107*, 204–212. [[CrossRef](#)]
95. Hua, C.; Wang, X.; Gao, X.; Zheng, H.; Han, X.; Chen, G. Experimental research on the start-up characteristics and heat transfer performance of pulsating heat pipes with rectangular channels. *Appl. Therm. Eng.* **2017**, *126*, 1058–1062. [[CrossRef](#)]
96. Wang, J.; Pan, Y.; Liu, X. Investigation on start-up and thermal performance of the single-loop pulsating heat pipe with variable diameter. *Int. J. Heat Mass Transf.* **2021**, *180*, 121811. [[CrossRef](#)]
97. Tseng, C.Y.; Yang, K.S.; Chien, K.H.; Jeng, M.S.; Wang, C. Investigation of the performance of pulsating heat pipe subject to uniform/alternating tube diameters. *Exp. Therm. Fluid Sci.* **2014**, *54*, 85–92. [[CrossRef](#)]
98. Markal, B.; Candere, A.C.; Avci, M.; Aydin, Q. Effect of double cross sectional ratio on performance characteristics of pulsating heat pipes. *Int. Commun. Heat Mass Transf.* **2021**, *127*, 105583. [[CrossRef](#)]
99. Markal, B.; Candere, A.; Avci, M.; Aydin, Q. Investigation of flat plate type pulsating heat pipes via flow visualization-assisted experiments: Effect of cross sectional ratio. *Int. Commun. Heat Mass Transf.* **2021**, *125*, 105289. [[CrossRef](#)]
100. Kim, Y.B.; Kim, H.; Sung, J. Investigation of thermal enhancement factor in micro pulsating heat exchanger using LIF visualization technique. *Int. J. Heat Mass Transf.* **2020**, *159*, 120121. [[CrossRef](#)]
101. Kwon, G.H.; Kim, S.J. Operational characteristics of pulsating heat pipes with a dual-diameter tube. *Int. J. Heat Mass Transf.* **2014**, *75*, 184–195. [[CrossRef](#)]
102. Kwon, G.H.; Kim, S.J. Experimental investigation on the thermal performance of a micro pulsating heat pipe with a dual-diameter channel. *Int. J. Heat Mass Transf.* **2015**, *89*, 817–828. [[CrossRef](#)]
103. Yang, K.S.; Cheng, Y.C.; Liu, M.C.; Shyu, J.C. Micro pulsating heat pipes with alternate microchannel widths. *Appl. Therm. Eng.* **2015**, *83*, 131–138. [[CrossRef](#)]
104. Tseng, C.Y.; Yang, K.S.; Chien, K.H.; Wu, S.K.; Wang, C.C. A novel double pipe pulsating heat pipe design to tackle inverted heat source arrangement. *Appl. Therm. Eng.* **2016**, *106*, 697–701. [[CrossRef](#)]
105. Sun, X.; Li, S.; Jiao, B.; Gan, Z.; Pfothenhauer, J.; Wang, B.; Zhao, Q.; Liu, D. Experimental study on hydrogen pulsating heat pipes under different number of turns. *Cryogenics* **2020**, *111*, 03174. [[CrossRef](#)]
106. Qian, N.; Fu, Y.; Marengo, M.; Chen, J.; Xu, H. Start-up timing behavior of single-loop oscillating heat pipes based on the second-order dynamic model. *Int. J. Heat Mass Transf.* **2020**, *147*, 118994. [[CrossRef](#)]
107. Mameli, M.; Marengo, M.; Zinna, S. Numerical model of a multi-turn closed loop pulsating heat pipe: Effects of the local pressure losses due to meanderings. *Int. J. Heat Mass Transf.* **2012**, *55*, 1036–1047. [[CrossRef](#)]
108. Spinato, G.; Borhani, N.; Thome, J.R. Operational regimes in a closed loop pulsating heat pipe. *Int. J. Therm. Sci.* **2016**, *102*, 78–88. [[CrossRef](#)]
109. Lee, J.; Joo, Y.; Kim, S.J. Effects of the number of turns and the inclination angle on the operating limit of micro pulsating heat pipes. *Int. J. Heat Mass Transf.* **2018**, *124*, 1172–1180. [[CrossRef](#)]
110. Noh, H.Y.; Kim, S.J. Thermal characterization and optimization of pulsating heat pipes operating in a circulation mode. *Int. J. Heat Mass Transf.* **2017**, *115*, 1234–1246. [[CrossRef](#)]
111. Kim, B.; Li, L.; Kim, J.; Kim, D. A study on thermal performance of parallel connected pulsating heat pipe. *Appl. Therm. Eng.* **2017**, *126*, 1063–1068. [[CrossRef](#)]
112. Kim, W.; Kim, S.J. Effect of reentrant cavities on the thermal performance of a pulsating heat pipe. *Appl. Therm. Eng.* **2018**, *133*, 61–69. [[CrossRef](#)]
113. Kang, Z.; Shou, D.; Fan, J. Numerical Study of a Novel Single-loop Pulsating Heat Pipe with Separating Walls within the Flow Channel. *Appl. Therm. Eng.* **2021**, *196*, 117246. [[CrossRef](#)]
114. Qu, J.; Guan, F.; Lv, Y.; Wang, Y. Experimental study on the heat transport capability of micro-grooved oscillating heat pipe. *Case Stud. Therm. Eng.* **2021**, *26*, 101210. [[CrossRef](#)]
115. Lim, J.; Kim, S.J. Effect of a channel layout on the thermal performance of a flat plate micro pulsating heat pipe under the local heating condition. *Int. J. Heat Mass Transf.* **2019**, *137*, 1232–1240. [[CrossRef](#)]

116. Kim, J.; Kim, S.J. Experimental investigation on the effect of the condenser length on the thermal performance of a micro pulsating heat pipe. *Appl. Therm. Eng.* **2018**, *130*, 439–448. [[CrossRef](#)]
117. Wang, J.; Ma, H.; Zhu, Q. Effects of the evaporator and condenser length on the performance of pulsating heat pipes. *Appl. Therm. Eng.* **2015**, *91*, 1018–1025. [[CrossRef](#)]
118. Sedighi, E.; Amarloo, A.; Shafii, B. Numerical and experimental investigation of flat-plate pulsating heat pipes with extra branches in the evaporator section. *Int. J. Heat Mass Transf.* **2018**, *126*, 431–441. [[CrossRef](#)]
119. Sedighi, E.; Amarloo, A.; Shafii, M.B. Experimental investigation of the thermal characteristics of single-turn pulsating heat pipes with an extra branch. *Int. J. Therm. Sci.* **2018**, *134*, 258–268. [[CrossRef](#)]
120. Kim, Y.B.; Song, H.W.; Sung, J. Flow behavior of rapid thermal oscillation inside an asymmetric micro pulsating heat exchanger. *Int. J. Heat Mass Transf.* **2018**, *120*, 923–929. [[CrossRef](#)]
121. Chiang, C.M.; Chien, K.H.; Chen, H.M.; Wang, C.C. Theoretical study of oscillatory phenomena in a horizontal closed-loop pulsating heat pipe with asymmetrical arrayed minichannel. *Int. Commun. Heat Mass Transf.* **2012**, *39*, 923–930. [[CrossRef](#)]
122. Okazaki, S.; Fuke, H.; Ogawa, H. Performance of circular Oscillating Heat Pipe for highly adaptable heat transfer layout. *Appl. Therm. Eng.* **2021**, *198*, 117497. [[CrossRef](#)]
123. Liu, X.; Chen, X.; Zhang, Z.; Chen, Y. Thermal performance of a novel dual-serpentine-channel flat-plate oscillating heat pipe used for multiple heat sources and sinks. *Int. J. Heat Mass Transf.* **2020**, *161*, 120293. [[CrossRef](#)]
124. Fonseca, L.D.; Pfothenauer, J.; Miller, F. Results of a three evaporator cryogenic helium Pulsating Heat Pipe. *Int. J. Heat Mass Transf.* **2018**, *120*, 1275–1286. [[CrossRef](#)]
125. Wang, J.; Ma, H.; Zhu, Q.; Dong, Y.; Yue, K. Numerical and experimental investigation of pulsating heat pipes with corrugated configuration. *Appl. Therm. Eng.* **2016**, *102*, 158–166. [[CrossRef](#)]
126. He, Y.; Jiao, D.; Pei, G.; Hu, X.; Hu, L. Experimental study on a three-dimensional pulsating heat pipe with tandem tapered nozzles. *Exp. Therm. Fluid Sci.* **2020**, *119*, 110201. [[CrossRef](#)]
127. Yeboah, S.K.; Darkwa, J. Experimental data on Helically Coiled Oscillating Heat Pipe (HCOHP) design and thermal performance. *Data Brief* **2020**, *33*, 106505. [[CrossRef](#)] [[PubMed](#)]
128. Ebrahimi, M.; Shafii, M.B.; Bijarchi, M.A. Experimental investigation of the thermal management of flat-plate closed-loop pulsating heat pipes with interconnecting channels. *Appl. Therm. Eng.* **2015**, *90*, 838–847. [[CrossRef](#)]
129. Qu, J.; Zhao, J.; Rao, Z. Experimental investigation on thermal performance of multi-layers three-dimensional oscillating heat pipes. *Int. J. Heat Mass Transf.* **2017**, *115*, 810–819. [[CrossRef](#)]
130. Qu, J.; Ke, Z.; Zuo, A.; Rao, Z. Experimental investigation on thermal performance of phase change material coupled with three-dimensional oscillating heat pipe (PCM/3D-OHP) for thermal management application. *Int. J. Heat Mass Transf.* **2019**, *129*, 773–782. [[CrossRef](#)]
131. Ando, M.; Okamoto, A.; Nagai, H. Start-up and heat transfer characteristics of oscillating heat pipe with different check valve layouts. *Appl. Therm. Eng.* **2021**, *196*, 117286. [[CrossRef](#)]
132. Ando, M.; Okamoto, A.; Tanaka, K.; Maeda, M.; Sugita, H.; Daimaru, T.; Nagai, H. On-orbit demonstration of oscillating heat pipe with check valves for space application. *Appl. Therm. Eng.* **2018**, *130*, 552–560. [[CrossRef](#)]
133. Fairley, J.D.; Thompson, S.M.; Anderson, D. Time–frequency analysis of flat-plate oscillating heat pipes. *Int. J. Therm. Sci.* **2015**, *91*, 113–124. [[CrossRef](#)]
134. De Vries, S.F.; Florea, D.; Homburg, F.G.A.; Frijns, A.J.H. Design and operation of a Tesla-type valve for pulsating heat pipes. *Int. J. Heat Mass Transf.* **2017**, *105*, 1–11. [[CrossRef](#)]
135. Thompson, S.M.; Ma, H.B.; Wilson, C. Investigation of a flat-plate oscillating heat pipe with Tesla-type check valves. *Exp. Therm. Fluid Sci.* **2011**, *35*, 1265–1273. [[CrossRef](#)]
136. Feng, C.; Wan, Z.; Mo, H.; Tang, H.; Lu, L.; Tang, Y. Heat transfer characteristics of a novel closed-loop pulsating heat pipe with a check valve. *Appl. Therm. Eng.* **2018**, *141*, 558–564. [[CrossRef](#)]
137. Bhuwakietkumjohn, N.; Rittidech, S. Internal flow patterns on heat transfer characteristics of a closed-loop oscillating heat-pipe with check valves using ethanol and a silver nano-ethanol mixture. *Exp. Therm. Fluid Sci.* **2010**, *34*, 1000–1007. [[CrossRef](#)]
138. Wan, Z.; Wang, X.; Feng, C. Heat transfer performances of the capillary loop pulsating heat pipes with spring-loaded check valve. *Appl. Therm. Eng.* **2020**, *167*, 114803. [[CrossRef](#)]
139. Daimaru, T.; Nagai, H.; Ando, M.; Tanaka, K.; Okamoto, A.; Sugita, H. Comparison between numerical simulation and on-orbit experiment of oscillating heat pipes. *Int. J. Heat Mass Transf.* **2017**, *109*, 791–806. [[CrossRef](#)]
140. Rahman, M.L.; Sultan, R.A.; Islam, T.; Hasan, N.M.; Ali, M. An experimental investigation on the effect of fin in the performance of closed loop pulsating heat pipe (CLPHP). *Procedia Eng.* **2015**, *105*, 137–144. [[CrossRef](#)]
141. Rahman, M.L.; Mir, F.; Nawrin, S.; Sultan, R.A.; Ali, M. Effect of fin and insert on the performance characteristics of Open Loop Pulsating Heat Pipe (OLPHP). *Procedia Eng.* **2015**, *105*, 105–112. [[CrossRef](#)]
142. Qu, J.; Li, X.; Wang, Q.; Liu, F.; Guo, H. Heat transfer characteristics of micro-grooved oscillating heat pipes. *Exp. Therm. Fluid Sci.* **2017**, *85*, 75–84. [[CrossRef](#)]
143. Odagiri, K.; Wolk, K.; Cappucci, S.; Morellina, S.; Roberts, S.; Pate, A.; Furst, B.; Sunada, E.; Daimaru, T. Three-dimensional heat transfer analysis of flat-plate oscillating heat pipes. *Appl. Therm. Eng.* **2021**, *195*, 117189. [[CrossRef](#)]
144. Der, O.; Alqahtani, A.A.; Marengo, M.; Bertola, V. Characterization of polypropylene pulsating heat stripes: Effects of orientation, heat transfer fluid, and loop geometry. *Appl. Therm. Eng.* **2021**, *184*, 116304. [[CrossRef](#)]

145. Arai, T.; Kawaji, M. Thermal performance and flow characteristics in additive manufactured polycarbonate pulsating heat pipes with Novec 7000. *Appl. Therm. Eng.* **2021**, *197*, 117273. [[CrossRef](#)]
146. Ibrahim, O.T.; Monroe, J.G.; Thompson, S.M.; Shamsaei, N.H.; Bilheux, A.; Elwany, A.; Biane, L. An investigation of a multi-layered oscillating heat pipe additively manufactured from Ti-6Al-4V powder. *Int. J. Heat Mass Transf.* **2017**, *108*, 1036–1047. [[CrossRef](#)]
147. Bhramara, P. CFD analysis of copper closed loop pulsating heat pipe. *Mater. Today Proc.* **2018**, *5*, 5487–5495.
148. Lim, J.; Kim, S.J. Fabrication and experimental evaluation of a polymer-based flexible pulsating heat pipe. *Energy Convers. Manag.* **2018**, *156*, 358–364. [[CrossRef](#)]
149. Qu, J.; Li, X.; Cui, Y.; Wang, Q. Design and experimental study on a hybrid flexible oscillating heat pipe. *Int. J. Heat Mass Transf.* **2017**, *107*, 640–645. [[CrossRef](#)]
150. Betancur, L.; Mangini, D.; Mantelli, M.; Marco, M. Experimental study of thermal performance in a closed loop pulsating heat pipe with alternating superhydrophobic channels. *Therm. Sci. Eng. Prog.* **2020**, *17*, 100360. [[CrossRef](#)]
151. Hao, T.; Ma, X.; Lan, Z.; Li, N.; Zhao, Y.; Ma, H. Effects of hydrophilic surface on heat transfer performance and oscillating motion for an oscillating heat pipe. *Int. J. Heat Mass Transf.* **2014**, *72*, 50–65. [[CrossRef](#)]
152. Betancur-Arboleda, L.A.; Mera, J.P.F.; Mantelli, M. Experimental study of channel roughness effect in diffusion bonded pulsating heat pipes. *Appl. Therm. Eng.* **2020**, *166*, 114734. [[CrossRef](#)]
153. Xie, K.; Ji, Y.; Yu, C.; Wu, C.; Yi, M. Experimental investigation on an aluminum oscillating heat pipe charged with water. *Appl. Therm. Eng.* **2019**, *162*, 114182. [[CrossRef](#)]
154. Taft, B.S.; Rhodes, M. Experimental investigation of oscillating heat pipes under direct current and pulse width modulation heating input conditions. *Appl. Therm. Eng.* **2017**, *126*, 1018–1022. [[CrossRef](#)]
155. Xian, H.; Xu, W.; Zhang, Y.; Du, X.; Yang, Y. Thermal characteristics and flow patterns of oscillating heat pipe with pulse heating. *Int. J. Heat Mass Transf.* **2014**, *79*, 332–341. [[CrossRef](#)]
156. Mangini, D.; Mameli, M.; Fioriti, D.; Filippeschi, S.; Araneo, L.; Marengo, M. Hybrid Pulsating Heat Pipe for space applications with non-uniform heating patterns: Ground and microgravity experiments. *Appl. Therm. Eng.* **2017**, *126*, 1029–1043. [[CrossRef](#)]
157. Jang, D.S.; Chung, H.J.; Jeon, Y.; Kim, Y. Thermal performance characteristics of a pulsating heat pipe at various nonuniform heating conditions. *Int. J. Heat Mass Transf.* **2018**, *126*, 855–863. [[CrossRef](#)]
158. Chen, X.; Chen, S.; Zhang, Z.; Kim, Y. Heat transfer investigation of a flat-plate oscillating heat pipe with tandem dual channels under nonuniform heating. *Int. J. Heat Mass Transf.* **2021**, *180*, 121830. [[CrossRef](#)]
159. Zhao, J.; Wu, C.; Rao, Z. Numerical study on heat transfer enhancement of closed loop oscillating heat pipe through active incentive method. *Int. Commun. Heat Mass Transf.* **2020**, *115*, 104612. [[CrossRef](#)]
160. Lim, J.; Kim, S.J. A channel layout of a micro pulsating heat pipe for an excessively localized heating condition. *Appl. Therm. Eng.* **2021**, *196*, 17266. [[CrossRef](#)]
161. Nine, M.J.; Tanshen, M.R.; Munkhbayar, B.; Chung, H.; Jeong, H. Analysis of pressure fluctuations to evaluate thermal performance of oscillating heat pipe. *Energy* **2014**, *70*, 135–142. [[CrossRef](#)]
162. Qu, J.; Zuo, A.; Liu, F.; Rao, Z. Quantitative analysis of thermal performance and flow characteristics of oscillating heat pipes with different initial pressure. *Appl. Therm. Eng.* **2020**, *181*, 115962. [[CrossRef](#)]
163. Yin, D.; Rajab, H.; Ma, H.B. Theoretical analysis of maximum filling ratio in an oscillating heat pipe. *Int. J. Heat Mass Transf.* **2014**, *74*, 353–357. [[CrossRef](#)]
164. Barua, H.; Ali, M.; Nuruzzaman, M.; Quamrul Islam, M.; Feroz, C. Effect of filling ratio on heat transfer characteristics and performance of a closed loop pulsating heat pipe. *Procedia Eng.* **2013**, *56*, 88–95. [[CrossRef](#)]
165. Fonseca, L.D.; Miller, F.; Pfothenauer, J. Experimental heat transfer analysis of a cryogenic nitrogen pulsating heat Pipe at various liquid fill ratios. *Appl. Therm. Eng.* **2018**, *130*, 343–353. [[CrossRef](#)]
166. Chien, K.H.; Lin, Y.T.; Chen, Y.R.; Yang, K.; Wang, C. A novel design of pulsating heat pipe with fewer turns applicable to all orientations. *Int. J. Heat Mass Transf.* **2012**, *55*, 5722–5728. [[CrossRef](#)]
167. Jang, D.S.; Lee, J.S.; Ahn, J.H.; Kim, D.; Kim, Y. Flow patterns and heat transfer characteristics of flat plate pulsating heat pipes with various asymmetric and aspect ratios of the channels. *Appl. Therm. Eng.* **2017**, *114*, 211–220. [[CrossRef](#)]
168. Li, M.; Li, L.; Xu, D. Effect of number of turns and configurations on the heat transfer performance of helium cryogenic pulsating heat pipe. *Cryogenics* **2018**, *96*, 159–165. [[CrossRef](#)]
169. Saha, N.; Das, P.K.; Sharma, P.K. Influence of process variables on the hydrodynamics and performance of a single loop pulsating heat pipe. *Int. J. Heat Mass Transf.* **2014**, *74*, 238–250. [[CrossRef](#)]
170. Ayel, V.; Slobodeniuk, M.; Bertossi, R.; Karmakar, A.; Martineau, F.; Romestant, C.; Bertin, Y.; Khandekar, S. Thermal performances of a Flat-Plate Pulsating Heat Pipe tested with water, aqueous mixtures and surfactants. *Int. J. Therm. Sci.* **2022**, *178*, 107599. [[CrossRef](#)]
171. Xing, M.; Yu, J.; Wang, R. Performance of a vertical closed pulsating heat pipe with hydroxylated MWNTs nanofluid. *Int. J. Heat Mass Transf.* **2017**, *112*, 81–88. [[CrossRef](#)]
172. Hashemi, S.M.; Maleki, A.; Ahmadi, M.H. The effect of some metal oxide nanocomposites on the pulsating heat pipe performance. *Energy Rep.* **2021**, *7*, 8825–8833. [[CrossRef](#)]

173. Czajkowski, C.; Nowak, A.I.; Błasiak, P.; Agnieszka, O.; Sławomir, P. Experimental study on a large scale pulsating heat pipe operating at high heat loads, different adiabatic lengths and various filling ratios of acetone, ethanol, and water. *Appl. Therm. Eng.* **2020**, *165*, 114534. [[CrossRef](#)]
174. Yeboah, S.K.; Darkwa, J. Experimental investigation into the integration of solid desiccant packed beds with oscillating heat pipes for energy efficient isothermal adsorption processes. *Therm. Sci. Eng. Prog.* **2021**, *21*, 100791. [[CrossRef](#)]
175. Chang, S.W.; Chen, G.W.; Lin, Y.P.; Liao, Y. Thermal performance of a cylindrical shell-like thin networked pulsating heat pipe. *Exp. Therm. Fluid Sci.* **2022**, *130*, 110524. [[CrossRef](#)]
176. Lee, Y.J.; Kim, S.J. Effects of the micro-post array on the maximum allowable input power for a micro pulsating heat pipe. *Int. J. Heat Mass Transf.* **2022**, *193*, 122898. [[CrossRef](#)]
177. Qian, N.; Fu, Y.; Chen, J.; Marengo, M.; Zhang, J.; Xua, J. Thermal performance analysis of axial-rotating oscillating heat pipe and its prediction model based on grey system theory. *Therm. Sci. Eng. Prog.* **2022**, *29*, 101210. [[CrossRef](#)]
178. Wang, X.; Li, B.; Yan, Y.; Gao, N.; Chen, G. Predicting of thermal resistances of closed vertical meandering pulsating heat pipe using artificial neural network model. *Appl. Therm. Eng.* **2019**, *149*, 1134–1141. [[CrossRef](#)]
179. Wang, X.; Yan, Y.; Meng, X.; Chen, G. A general method to predict the performance of closed pulsating heat pipe by artificial neural network. *Appl. Therm. Eng.* **2019**, *157*, 13761. [[CrossRef](#)]
180. Chu, L.; Ji, Y.; Liu, Z.; Yu, C.; Wu, Z.; Wang, Z.; Yang, Y.; Yang, X. Structure optimization of a three-dimensional coil oscillating heat pipe. *Int. J. Heat Mass Transf.* **2022**, *183*, 122229. [[CrossRef](#)]
181. Min, C.; Gao, X.; Li, F.; Wang, K. Thermal performance analyses of pulsating heat pipe for application in proton exchange member fuel cell. *Energy Convers. Manag.* **2022**, *259*, 115566. [[CrossRef](#)]
182. Kang, Z.; Shou, D.; Fan, J. Numerical study of single-loop pulsating heat pipe with porous wicking layer. *Int. J. Therm. Sci.* **2022**, *179*, 107614. [[CrossRef](#)]
183. Qian, N.; Fu, Y.; Khan, A.M.; Ding, W.; Jiang, F.; Zhang, J.; Xu, J. Holistic sustainability assessment of novel oscillating-heat-pipe grinding-wheel in Earth-friendly abrasive machining. *J. Clean. Prod.* **2022**, *352*, 131486. [[CrossRef](#)]
184. Monroe, J.G.; Ibrahim, O.T.; Thompson, S.M. Effect of harvesting module design on the thermal performance and voltage generation of a thermoelectric oscillating heat pipe. *Appl. Therm. Eng.* **2022**, *201*, 117651. [[CrossRef](#)]
185. Aref, L.; Fallahzadeh, R.; Avargani, V.M. An experimental investigation on a portable bubble basin humidification/dehumidification desalination unit utilizing a closed-loop pulsating heat pipe. *Energy Convers. Manag.* **2021**, *228*, 113694. [[CrossRef](#)]
186. Khalilmoghadam, P.; Rajabi-Ghahnavieh, A.; Shafii, M.B. A novel energy storage system for latent heat recovery in solar still using phase change material and pulsating heat pipe. *Renew. Energy* **2021**, *163*, 2115–2127. [[CrossRef](#)]
187. Barba, M.; Bruce, R.; Bouchet, F.; Bonelli, A.; Baudouy, B. Effect of the thermo-physical properties of the working fluid on the performance of a 1-m long cryogenic horizontal pulsating heat pipe. *Int. J. Heat Mass Transf.* **2022**, *187*, 122458. [[CrossRef](#)]
188. Yasuda, Y.; Nabeshima, F.; Horiuchi, K.; Nagai, H. Visualization of the working fluid in a flat-plate pulsating heat pipe by neutron radiography. *Int. J. Heat Mass Transf.* **2022**, *185*, 122336. [[CrossRef](#)]
189. Wang, J.; Xie, J.; Liu, X. Investigation of wettability on performance of pulsating heat pipe. *Int. J. Heat Mass Transf.* **2020**, *150*, 119354. [[CrossRef](#)]
190. Xu, R.; Li, X.; Lei, T.; Wu, Q.; Wang, R. Operation characteristics of a gravity pulsating heat pipe under different heat inputs. *Int. J. Heat Mass Transf.* **2022**, *189*, 122731. [[CrossRef](#)]
191. Chen, X.; Liu, X.; Xu, D.; Chen, Y. Thermal performance of a tandem-dual-channel flat-plate pulsating heat pipe applicable to hypergravity. *Int. J. Heat Mass Transf.* **2022**, *189*, 122656. [[CrossRef](#)]
192. Abela, M.; Mameli, M.; Nikolayev, V.; Filippeschi, S. Experimental analysis and transient numerical simulation of a large diameter pulsating heat pipe in microgravity conditions. *Int. J. Heat Mass Transf.* **2022**, *187*, 122532. [[CrossRef](#)]
193. Li, S.; Sun, X.; Liu, D. Experimental study on a hydrogen pulsating heat pipe in different heating modes. *Cryogenics* **2022**, *123*, 103440. [[CrossRef](#)]
194. Qian, N.; Fu, Y.; Jiang, F.; Ding, W.; Zhang, J.; Xu, J. CBN grain wear during eco-benign grinding of nickel-based superalloy with oscillating heat pipe abrasive wheel. *Ceram. Int.* **2022**, *48*, 9692–9701. [[CrossRef](#)]
195. Wu, Z.; Xing, Y.; Liu, L.; Huang, P.; Zhao, G. Design, fabrication and performance evaluation of pulsating heat pipe assisted tool holder. *J. Manuf. Processes* **2020**, *50*, 224–233. [[CrossRef](#)]
196. Senjaya, R.; Inoue, T. Effects of non-condensable gas on the performance of oscillating heat pipe, part I: Theoretical study. *Appl. Therm. Eng.* **2014**, *73*, 1387–1392. [[CrossRef](#)]
197. Kamijima, C.; Yoshimoto, Y.; Abe, Y.; Takagi, A.; Kinefuchi, I. Relating the thermal properties of a micro pulsating heat pipe to the internal flow characteristics via experiments, image recognition of flow patterns and heat transfer simulations. *Int. J. Heat Mass Transf.* **2020**, *163*, 120415. [[CrossRef](#)]
198. Lin, Z.; Wang, S.; Chen, J.; Huo, J.; Hu, Y.; Zhang, W. Experimental study on effective range of miniature oscillating heat pipes. *Appl. Therm. Eng.* **2011**, *31*, 880–886. [[CrossRef](#)]
199. Sun, Q.; Qu, J.; Yuan, J.; Wang, Q. Operational characteristics of an MEMS-based micro oscillating heat pipe. *Appl. Therm. Eng.* **2017**, *124*, 1269–1278. [[CrossRef](#)]
200. Aref, L.; Fallahzadeh, R.; Shabanian, S.R.; Hosseinzadeh, M. A novel dual-diameter closed-loop pulsating heat pipe for a flat plate solar collector. *Energy* **2021**, *230*, 120751. [[CrossRef](#)]

201. Zhao, J.; Jiang, W.; Rao, Z. Operational characteristics of oscillating heat pipe with long heat transport distance for solar energy application. *Exp. Therm. Fluid Sci.* **2018**, *98*, 137–145. [[CrossRef](#)]
202. Jin, H.; Lin, G.; Zeiny, A.; Bai, L.; Cai, J.; Wen, D. Experimental study of transparent oscillating heat pipes filled with solar absorptive nanofluids. *Int. J. Heat Mass Transf.* **2019**, *139*, 189–801. [[CrossRef](#)]
203. Zhao, J.; Qu, J.; Rao, Z. Experiment investigation on thermal performance of a large-scale oscillating heat pipe with self-rewetting fluid used for thermal energy storage. *Int. J. Heat Mass Transf.* **2017**, *108*, 760–769. [[CrossRef](#)]
204. Qu, J.; Zuo, A.; Liu, H.; Zhao, J.; Rao, Z. Three-dimensional oscillating heat pipes with novel structure for latent heat thermal energy storage application. *Appl. Therm. Eng.* **2021**, *187*, 116574. [[CrossRef](#)]
205. Chen, X.; Shao, S.; Xiang, J.; Xiang, J.; Ma, W.; Zhang, H. Experimental investigation on ethane pulsating heat pipe based on Stirling cooler. *Int. J. Refrig.* **2018**, *88*, 506–515. [[CrossRef](#)]
206. Xu, X.; Zhang, X. Finite time thermodynamics analysis and research of pulsating heat pipe cold storage device. *Energy Storage Sav.* **2022**, *1*, 33–43. [[CrossRef](#)]
207. Saw, L.H.; Yew, M.C.; Yew, M.K.; Chong, W.T.; Poon, H.M.; Liew, W.S.; Yeo, W.H. Development of the closed loop pulsating heat pipe cool roof system for residential buildings. *Case Stud. Therm. Eng.* **2021**, *28*, 101487. [[CrossRef](#)]